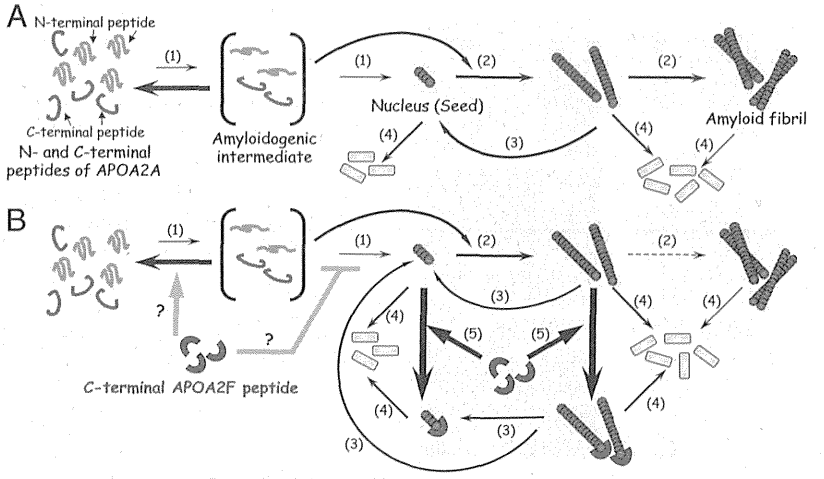

Fig. 9. Models showing amyloid fibril formation by apoA-II protein and the selective inhibition by the C-terminal APOA2F peptide. (*A*) Amyloid fibril formation of apoA-II peptides in vitro (23). N- and C-terminal APOA2A peptides change their secondary structures under acidic conditions (pH 2.5) with amyloidogenic conformation (intermediate) and polymerize into a nucleus (seed) (step 1). Once a nucleus is formed, or new nuclei (seeds) are made by fragmentation of amyloid fibrils, further extension of amyloidogenic peptides occurs (steps 2 and 3). Amyloid fibrils are degraded in the course of time, except for the supply of combination of N- and C-terminal amyloidogenic peptides (step 4). (*B*) Hypothetical mechanism by which the C-terminal APOA2F peptide inhibits amyloid fibril formation. The C-terminal APOA2F peptide strongly inhibits the extension phase of amyloidogenic peptides by capping possible active ends of seeds (step 5). As a result, amyloidogenic APOA2A peptides cannot polymerize into amyloid fibrils (step 2).

Microscopic Analyses of the Experiments Using Synthetic Peptides. For TEM experiments, we prepared the sample according to methods described previously (23). The reaction mixtures were spread on carbon-coated grids (400 mesh; NEM) and were negatively stained with 1% (wt/vol) phosphotungstic acid (electron microscopy grade; TAAB Laboratories Equipment Ltd.)-NaOH (pH 7.0). These samples were examined under an electron microscope (1200EX or 1400EX; JEOL) with an acceleration voltage of 80 kV. Immunoelectron microscopy was performed using a modified method in parts described previously (51). The preincubated seeds with biotin-labeled a48/65 (N62K) were resuspended in the reaction solution and recentrifuged. Pellets were resuspended again and loaded immediately onto carbon-coated grids at room temperature (25 °C) for 15 min. The grids were immersed in 1:4 streptavidin-conjugated 10 nm colloidal gold (EM.STP10; BBI Solutions) in 50 mM phosphate buffer (pH 7.0) containing 0.5% BSA and 0.05% Tween 20. After 3 h at 25 °C, the grids were washed twice using phosphate buffer and then negatively stained with 1% phosphotungstic acid-NaOH (pH 7.0). The grids were observed under an electron microscope 1400EX.

For LM observations, the reaction mixtures were applied to silanized glass slides (S3003; DAKO Cytomation Co.), dried overnight in a 37 °C dry box, and stained with 1% Congo red dye (23). These samples were examined for apple-green colored birefringence under polarized light using a LM.

LC-MS/MS Analysis. Aliquots of reaction mixtures were centrifuged, and the pellets were stored in a −80 °C freezer immediately after the supernatants were removed. The pellets were redissolved in 99% formic acid and diluted with 2% (vol/vol) formic acid/2% (vol/vol) acetonitrile, and analyzed by LC-MS/MS as described previously (23, 52). The sample solutions were applied to a Paradigm MS4 (Microm BioResources, Inc.) HPLC system fitted with an HTC-PAL automatic sampler (CHROMSYS LLC). A reverse-phase capillary column (Develosil ODS-HG3, 0.075 mm i.d. × 50 mm; Nomura Chemical Co. Ltd.) was used at a flow rate of 200 nL/min with a 4–72% (vol/vol) linear gradient of acetonitrile in 0.1% formic acid. Eluted apoA-II partial peptides were directly detected with an ion trap mass spectrometer, LXQ (Thermo Electron Corporation). The data were analyzed with SEQUEST (Thermo Electron Corporation).

Suppression of AApoAII Amyloidosis in Mice by the C-Terminal Peptide of apoA-II. Osmotic pumps (ALZET micro-osmotic pump, no. 1004; DURECT Corp.) were filled with 1.0 mM a48/65(N62K) or a48/65 peptide solutions in 5% (vol/vol) DMSO or vehicle according to the manufacturer's instructions. Two-month-old *Apoa2*^{c}-*Tg*$^{+/-}$ mice were anesthetized with pentobarbital sodium (Somnopentyl; Kyoritsu Seiyaku Corp.), and the osmotic pumps were implanted into their abdominal cavities. One day after the implantation, the mice were injected i.v. with 5 μg of sonicated AApoAII fibrils. After 27 d, the mice were killed by cardiac puncture under deep anesthesia using diethyl ether. Several organs were collected and used to detect amyloid deposits.

Chemical Reagents. Unless otherwise specified, chemical reagents in this section were obtained from Wako Pure Chemical Industries, Ltd.

Statistical Analysis. We used the R software package (The R Development Core Team, Vienna University of Economics and Business). The Mann–Whitney *U* test was used to analyze the AI for amyloid deposits. The Tukey–Kramer method for multiple comparisons was performed to test for any significant differences in various pairwise comparisons in blood biochemical parameters. The Student's *t* test was used to analyze the inhibitory abilities of the C-terminal peptides on polymerization of APOA2A peptides. The one-way ANOVA was used to test for any significant differences in the stability of amyloid fibrils in the presence of additional C-terminal peptides. *P* values <0.05 were regarded as statistically significant.

ACKNOWLEDGMENTS. We thank Prof. Kiyoshi Matsumoto, Ms. Ayako Nishio, Mr. Kiyokazu Kametani, and Ms. Kayo Suzuki (Research Support Center for Human and Environmental Sciences, Shinshu University) for animal care and technical assistance with TEM. We greatly appreciate the helpful suggestions and comments from Prof. Yuji Goto (Osaka University) and Prof. Vittorio Bellotti (University of Pavia). This research was supported in part by Grants-in-Aid for Priority Areas (22020015) and Scientific Research (B) (20300144, 23390093, and 26293084) from the Ministry of Education, Culture, Sports, Science and Technology, Japan, and by grants for the Amyloidosis Research Committee from the Ministry of Health, Labour and Welfare, Japan.

1. Kelly JW (1998) The alternative conformations of amyloidogenic proteins and their multi-step assembly pathways. *Curr Opin Struct Biol* 8(1):101–106.
2. Westermark P, et al. (2002) Amyloid fibril protein nomenclature: 2002. *Amyloid* 9(3): 197–200.
3. Nguyen HD, Hall CK (2004) Molecular dynamics simulations of spontaneous fibril formation by random-coil peptides. *Proc Natl Acad Sci USA* 101(46):16180–16185.
4. Lindgren M, Sörgjerd K, Hammarström P (2005) Detection and characterization of aggregates, prefibrillar amyloidogenic oligomers, and protofibrils using fluorescence spectroscopy. *Biophys J* 88(6):4200–4212.
5. Olzscha H, et al. (2011) Amyloid-like aggregates sequester numerous metastable proteins with essential cellular functions. *Cell* 144(1):67–78.
6. Tjernberg L, Hosia W, Bark N, Thyberg J, Johansson J (2002) Charge attraction and β propensity are necessary for amyloid fibril formation from tetrapeptides. *J Biol Chem* 277(45):43243-43246.
7. Stefani M, Dobson CM (2003) Protein aggregation and aggregate toxicity: New insights into protein folding, misfolding diseases and biological evolution. *J Mol Med (Berl)* 81(11):678–699.
8. Selkoe DJ (2004) Cell biology of protein misfolding: The examples of Alzheimer's and Parkinson's diseases. *Nat Cell Biol* 6(11):1054–1061.

9. Xing Y, Higuchi K (2002) Amyloid fibril proteins. *Mech Ageing Dev* 123(12): 1625–1636.
10. Sekijima Y, et al. (2005) The biological and chemical basis for tissue-selective amyloid disease. *Cell* 121(1):73–85.
11. Blanco-Vaca F, Escolà-Gil JC, Martín-Campos JM, Julve J (2001) Role of apoA-II in lipid metabolism and atherosclerosis: Advances in the study of an enigmatic protein. *J Lipid Res* 42(11):1727–1739.
12. Higuchi K, et al. (1986) Purification and characterization of a senile amyloid-related antigenic substance (apoSAS$_{SAM}$) from mouse serum: apoSASSAM is an apoA-II apolipoprotein of mouse high density lipoproteins. *J Biol Chem* 261(27):12834–12840.
13. Xing Y, et al. (2002) Induction of protein conformational change in mouse senile amyloidosis. *J Biol Chem* 277(36):33164–33169.
14. Zhang H, et al. (2006) Transmissibility of mouse AApoAII amyloid fibrils: Inactivation by physical and chemical methods. *FASEB J* 20:1012–1014.
15. Ge F, et al. (2007) Amyloidosis in transgenic mice expressing murine amyloidogenic apolipoprotein A-II (*Apoa2^c*). *Lab Invest* 87(7):633–643.
16. Kitagawa K, et al. (2003) Polymorphisms of mouse apolipoprotein A-II: Seven alleles found among 41 inbred strains of mice. *Amyloid* 10(4):207–214.
17. Higuchi K, Yonezu T, Tsunasawa S, Sakiyama F, Takeda T (1986) The single proline-glutamine substitution at position 5 enhances the potency of amyloid fibril formation of murine apo A-II. *FEBS Lett* 207(1):23–27.
18. Fu X, et al. (2004) Induction of AApoAII amyloidosis by various heterogeneous amyloid fibrils. *FEBS Lett* 563(1-3):179–184.
19. Higuchi K, et al. (1991) Polymorphism of apolipoprotein A-II (apoA-II) among inbred strains of mice: Relationship between the molecular type of apoA-II and mouse senile amyloidosis. *Biochem J* 279(Pt 2):427–433.
20. Higuchi K, Naiki H, Kitagawa K, Hosokawa M, Takeda T (1991) Mouse senile amyloidosis: AS$_{SAM}$ amyloidosis in mice presents universally as a systemic age-associated amyloidosis. *Virchows Arch B Cell Pathol Incl Mol Pathol* 60(4):231–238.
21. HogenEsch H, et al. (1993) Gastrointestinal AAPOAII and systemic AA-amyloidosis in aged C57BL/Ka mice: Amyloid-type dependent effect of long-term immunosuppressive treatment. *Virchows Arch B Cell Pathol Incl Mol Pathol* 64(1):37–43.
22. Gruys E, Tooten PCJ, Kuijpers MHM (1996) Lung, ileum and heart are predilection sites for AApoAII amyloid deposition in CD-1 Swiss mice used for toxicity studies: Pulmonary amyloid indicates AApoAII. *Lab Anim* 30(1):28–34.
23. Sawashita J, et al. (2009) Amyloid fibrils formed by selective N-, C-terminal sequences of mouse apolipoprotein A-II. *Biochim Biophys Acta* 1794(10):1517–1529.
24. Hasegawa K, Yamaguchi I, Omata S, Gejyo F, Naiki H (1999) Interaction between A β(1-42) and A β(1-40) in Alzheimer's β-amyloid fibril formation in vitro. *Biochemistry* 38(47):15514–15521.
25. Kozhukh GV, et al. (2002) Investigation of a peptide responsible for amyloid fibril formation of β_2-microglobulin by *achromobacter* protease I. *J Biol Chem* 277(2): 1310–1315.
26. Modler AJ, et al. (2004) Polymerization of proteins into amyloid protofibrils shares common critical oligomeric states but differs in the mechanisms of their formation. *Amyloid* 11(4):215–231.
27. Kammerer RA, et al. (2004) Exploring amyloid formation by a *de novo* design. *Proc Natl Acad Sci USA* 101(13):4435–4440.
28. Nguyen HD, Hall CK (2005) Kinetics of fibril formation by polyalanine peptides. *J Biol Chem* 280(10):9074–9082.
29. Higuchi K, et al. (1998) Fibrilization in mouse senile amyloidosis is fibril conformation-dependent. *Lab Invest* 78(12):1535–1542.
30. Higuchi K, et al. (1983) Systemic senile amyloid in senescence-accelerated mice: A unique fibril protein demonstrated in tissues from various organs by the unlabeled immunoperoxidase method. *Lab Invest* 48(2):231–240.
31. Korenaga T, et al. (2004) Tissue distribution, biochemical properties, and transmission of mouse type A AApoAII amyloid fibrils. *Am J Pathol* 164(5):1597–1606.
32. Wang Y, et al. (2011) ApoA-I deficiency in mice is associated with redistribution of apoA-II and aggravated AApoAII amyloidosis. *J Lipid Res* 52(8):1461–1470.
33. Higuchi K, et al. (1996) Accelerated senile amyloidosis induced by amyloidogenic Apoa-II gene shortens the life span of mice but does not accelerate the rate of senescence. *J Gerontol A Biol Sci Med Sci* 51(4):B295–B302.
34. Higuchi K, et al. (1993) Development of congenic strains of mice carrying amyloidogenic apolipoprotein A-II (Apoa2^c): Apoa2c reduces the plasma level and the size of high density lipoprotein. *FEBS Lett* 317(3):207–210.
35. Suto J, Takahashi Y, Sekikawa K (2004) Quantitative trait locus analysis of plasma cholesterol and triglyceride levels in C57BL/6J x RR F2 mice. *Biochem Genet* 42(9-10): 347–363.
36. Yonezu T, et al. (1987) A molecular-pathologic approach to murine senile amyloidosis: Serum precursor-apolipoprotein A-II variant (Pro^5——Gln) presents only in the senile amyloidosis-prone SAM-P/1 and SAM-P/2 mice. *Lab Invest* 57(1):65–70.
37. Valleix S, et al. (2012) Hereditary systemic amyloidosis due to Asp76Asn variant β_2-microglobulin. *N Engl J Med* 366(24):2276–2283.
38. Biasini E, et al. (2010) The hydrophobic core region governs mutant prion protein aggregation and intracellular retention. *Biochem J* 430(3):477–486.
39. Tzotzos S, Doig AJ (2010) Amyloidogenic sequences in native protein structures. *Protein Sci* 19(2):327–348.
40. Torbeev VY, Hilvert D (2013) Both the *cis-trans* equilibrium and isomerization dynamics of a single proline amide modulate β_2-microglobulin amyloid assembly. *Proc Natl Acad Sci USA* 110(50):20051–20056.
41. Alexandrescu AT (2013) Amide proton solvent protection in amylin fibrils probed by quenched hydrogen exchange NMR. *PLoS ONE* 8(2):e56467.
42. Pawar AP, et al. (2005) Prediction of "aggregation-prone" and "aggregation-susceptible" regions in proteins associated with neurodegenerative diseases. *J Mol Biol* 350(2):379–392.
43. Tartaglia GG, et al. (2008) Prediction of aggregation-prone regions in structured proteins. *J Mol Biol* 380(2):425–436.
44. Tartaglia GG, Vendruscolo M (2008) The Zyggregator method for predicting protein aggregation propensities. *Chem Soc Rev* 37(7):1395–1401.
45. Hamada D, et al. (2009) Competition between folding, native-state dimerisation and amyloid aggregation in β-lactoglobulin. *J Mol Biol* 386(3):878–890.
46. Fu L, et al. (2001) Extrahepatic expression of apolipoprotein A-II in mouse tissues: Possible contribution to mouse senile amyloidosis. *J Histochem Cytochem* 49(6): 739–748.
47. Pras M, Zucker-Franklin D, Rimon A, Franklin EC (1969) Physical, chemical, and ultrastructural studies of water-soluble human amyloid fibrils: Comparative analyses of nine amyloid preparations. *J Exp Med* 130(4):777–796.
48. Puchtler H, Sweat F, Levine M (1962) On the binding of Congo red by amyloid. *J Histochem Cytochem* 10:355–364.
49. Ravid M, Gafni J, Sohar E, Missmahl H-P (1967) Incidence and origin of non-systemic microdeposits of amyloid. *J Clin Pathol* 20(1):15–20.
50. Naiki H, Higuchi K, Hosokawa M, Takeda T (1989) Fluorometric determination of amyloid fibrils in vitro using the fluorescent dye, thioflavin T1. *Anal Biochem* 177(2): 244–249.
51. Yan J, et al. (2007) Cross-seeding and cross-competition in mouse apolipoprotein A-II amyloid fibrils and protein A amyloid fibrils. *Am J Pathol* 171(1):172–180.
52. Kametani F (2004) Secretion of long Abeta-related peptides processed at ε-cleavage site is dependent on the α-secretase pre-cutting. *FEBS Lett* 570(1-3):73–76.

Neurobiology of Aging 36 (2015) 634–637

Contents lists available at ScienceDirect

Neurobiology of Aging

journal homepage: www.elsevier.com/locate/neuaging

Brief communication

Accumulation of carboxy-terminal fragments of APP increases phosphodiesterase 8B

Fuyuki Kametani*, Seiichi Haga

Department of Dementia and Higher Brain Function, Tokyo Metropolitan Institute of Medical Science, Tokyo, Japan

ARTICLE INFO

Article history:
Received 7 April 2014
Received in revised form 19 September 2014
Accepted 30 September 2014
Available online 7 October 2014

Keywords:
Alzheimer's disease
Amyloid
APP
CTF
Aβ
Phosphodiesterase
cAMP
Proteomics

ABSTRACT

The long-standing "amyloid hypothesis" that Alzheimer's disease is caused by the production and aggregation of amyloid-β faces serious challenges by data recently obtained from neuroimaging studies and amyloid-β amyloid-focused clinical trials. Meanwhile, accumulation of carboxy-terminal fragments (CTFs) of the amyloid precursor protein (APP) may be neurotoxic and may impair synaptic plasticity and long-term memory in Alzheimer's disease, as suggested in murine models. To clarify these issues, we carried out a proteomic analysis of Chinese hamster ovary cells expressing APP CTFs and found that APP-CTF accumulation induced an increase in the level of phosphodiesterase 8B, suggesting that the hydrolysis of cyclic AMP was enhanced.

1. Introduction

According to the widely accepted amyloid hypothesis, amyloid-β (Aβ) production from amyloid precursor protein (APP) (Supplementary Fig. 1) and amyloid formation are considered the primary causes of Alzheimer's disease (AD). However, Aβ peptides are normal components, and there is little evidence that Aβ is neurotoxic at in vivo concentrations (Robakis, 2011). Recent neuroimaging studies have revealed that amyloid deposits are present in cognitively normal individuals, whereas some AD patients show no amyloid deposits in positron emission tomography analysis (Edison et al., 2007; Li et al., 2008). Furthermore, all Aβ amyloid-focused clinical trials have failed (Giacobini and Gold, 2013). The amyloid hypothesis seems not to be viable.

It has already been reported that accumulation of APP C-terminal fragments (CTFs, C83, C89, and C99 as shown in Supplementary Fig. 1), in particular C99, may be neurotoxic by itself, and that APP CTFs are able to impair synaptic plasticity and long-term memory in murine models of AD (Jiang et al., 2010; Kim et al., 2003; Lauritzen et al., 2012; Ohkawara et al., 2011; Oster-Granite et al., 1996; Passer et al., 2000). Recently, accumulation of APP CTFs was found in the AD brain (Pera et al., 2013). To understand the influence of APP-CTF accumulation, we carried out a proteomic analysis of Chinese hamster ovary (CHO) cells expressing APP CTFs and found that APP-CTF accumulation induced increased levels of phosphodiesterase 8B (PDE8B), suggesting that APP-CTF accumulation enhanced the hydrolysis of cyclic AMP (cAMP).

2. Methods

2.1. Extraction from CHO cells, digestion of trypsin, and labeling with iTRAQ reagents

CHO cells expressing APP CTFs (C83 and C89) and CHO cell transfected vector (mock) were cultured as described in the Supplementary Materials. To analyze the metabolism of APP CTF, Complete Lysis-M extracts (50 μg) were added to 6 volumes of −20 °C acetone and incubated at −20 °C for 3 hours. The resulting acetone precipitations were dissolved in 0.5 M triethylammonium bicarbonate in 0.1% SDS solution at pH 8.5 to which 100 nmol of tris-(2-carboxyethyl)phosphine was added. The mixtures were incubated at 60 °C for 1 hour, and 1 μL of 200 mM methyl methane-thiosulfonate was added in isopropanol and incubated at room temperature for 10 minutes. Thereafter, the mixtures were

* Corresponding author at: Department of Dementia and Higher Brain Function, Tokyo Metropolitan Institute of Medical Science, 2-1-6 Kamikitazawa, Setagaya-ku, Tokyo 156-8506, Japan. Tel.: +81 3 6834 2349; fax: +81 3 6834 2349.
E-mail address: kametani-fy@igakuken.or.jp (F. Kametani).

0197-4580/$ – see front matter © 2015 Elsevier Inc. All rights reserved.
http://dx.doi.org/10.1016/j.neurobiolaging.2014.09.029

digested with 10 μg of trypsin at 37 °C for 20 hours. The digests were labeled with iTRAQ reagent (AB SCIEX, Framingham, MA, USA) as described in the manufacturer's instructions. Briefly, the iTRAQ reagent was mixed with ethanol (30:70) at room temperature. After vortexing and spinning, each of the reagents was transferred to one tryptic digest. These digests were incubated at room temperature for 1 hour. The digests from mock CHO cells, CHO cells expressing C83, and CHO cells expressing C89 were labeled with 115, 116, and 117 regents, respectively. All iTRAQ reagent-labeled samples were combined and evaporated.

2.2. Liquid chromatography with ion trap spectrometry analysis

iTRAQ-labeled tryptic peptides were dissolved in 1 mL of 10 mM potassium phosphate in 25% acetonitrile at pH 3.0, loaded on a POROS 50 HS column (4 mm × 15 mm, AB SCIEX) and eluted with 0, 105, 175, 350, and 1000 mM potassium chloride in 10 mM potassium phosphate and 25% acetonitrile at pH 3.0. The eluted peptides were further resolved by a reverse-phase column (Develosil ODS-HG5, 0.075 mm × 150 mm, Nomura Chemical Co, Ltd, Seto, Japan). The peptides were eluted at a flow rate of 300 nL/min with a 2%–80% linear gradient of acetonitrile in 0.1% TFA. Eluted peptides were directly analyzed with an ion trap mass spectrometer, Velos Pro (Thermo Fisher Scientific Inc, Waltham, MA, USA) at a spray voltage of 1.9 kV and collision energy of 35%. An Mass Spectrum (MS) scan range of 400–2000 m/z was used in the positive ion mode, followed by data-dependent MS/MS using both HCD and CID operating modes on the top 5 ions in the order of abundance. Settings specific to HCD were a Q activation setting optimized at 0.08, a normalized collision energy of 45, and an activation time of 2.0 ms. The eluted peptides data were analyzed and combined with BioWorks (Thermo Fisher Scientific Inc). The value of false discovery rate was ≤0.05.

3. Results and discussion

APP CTFs are known to be metabolized in the γ-secretase–processing pathway and the endosome-lysosome pathway (Asai et al., 2011; Kametani, 2008). We confirmed this as described in Supplementary Fig. 2A. Under normal conditions, a small amount of APP CTFs were seen, suggesting that the levels of APP CTFs were strictly regulated. DAPT or NH_4Cl treatment significantly induced accumulations of APP CTFs, indicating that both endogenous and overexpressed APP were metabolized through these pathways.

Next, we analyzed APP intracellular domain (AICD) that was produced by ε-site cleavage near the cytoplasmic membrane boundary of APP CTFs via the γ-secretase processing pathway (Supplementary Fig. 1B). AICD regulates transcriptional stimulators or repressors (Chen and Selkoe, 2007; Marambaud et al., 2003; Pardossi-Piquard et al., 2005, 2007) and is rapidly metabolized (Cupers et al., 2001; Kopan and Ilagan, 2004).

C83 preferentially cleaved at the ε-site, whereas C89 and C99 faintly cleaved at the ε-site in CHO cells expressing APP CTFs, C83, C89, and C99 (Supplementary Fig. 2B). Recently, others have reported that C99 is an insufficient substrate for ε-site cleavage of γ-secretase (Funamoto et al., 2013), thereby supporting our results. Furthermore, the expressed AICD is rapidly degraded (Supplementary Fig. 3), as described previously (Cupers et al., 2001; Kopan and Ilagan, 2004). These findings suggest that APP CTFs, in particular the intracellular region (AICD), may be toxic and need to be removed (Kametani, 2008; Robakis and Georgakopoulos, 2013). To degrade the intracellular region, ε-site cleavage by γ-secretase may be indispensable.

Table 1
Expression levels of upregulated and downregulated proteins in CHO cells expressing C83 or C89

Protein names	CHO cell (fold)	
	C83	C89
APP (transfected C83 or C89)	5.6	4.5
High affinity cAMP-specific and IBMX-insensitive 3′,5′-cyclic phosphodiesterase 8B	4.6	6.7
Spermatogenesis-associated protein 2	2.6	3.6
Zinc finger protein PLAG1	2.3	3.0
Baculoviral inhibitors of apoptosis repeat-containing protein 1a	2.3	2.6
Lupus La protein homolog	2.2	2.3
Eukaryotic translation initiation factor 2 subunit 1	0.4	0.3
Prelamin-A/C	0.4	0.4
ATP-dependent RNA helicase DDX1	0.8	0.4
Histone H2A	0.5	0.4
Ubiquitin thioesterase OTUB1	0.4	0.7
Catalase	0.4	0.5
Heat shock protein 75 kDa, mitochondrial	0.4	0.5
Fibroblast growth factor 12	0.3	0.8
DNA-binding protein A	0.3	0.7
Sodium/potassium-transporting ATPase subunit alpha-1	0.2	0.6
Transitional endoplasmic reticulum ATPase valosin-containing protein	0.2	0.7

The expression level of these proteins from wild (mock) CHO cell is defined as 1.
Key: APP, amyloid precursor protein; ATP, adenosine triphosphate; cAMP, cyclic AMP; CHO, Chinese hamster ovary.

To analyze the influence of APP-CTF accumulation without Aβ involvement, we used CHO cells expressing C83 and C89 (Supplementary Fig. 1). These cell extracts were labeled with iTRAQ regent and analyzed by a proteomic method. We found that APP and PDE8B significantly increased in these CHO cells and that ATPases significantly decreased in CHO cells expressing C83 (Table 1 and Supplementary Excel file). CHO cells expressing C83, APP, and PDE8B showed 5.6- and 4.6-fold expression, respectively. CHO cells expressing C89, APP and PDE8B showed 4.5- and 6.7-fold expression, respectively. APP increases were because of overexpression of C83 or C89, respectively. Increase of PDE8b was apparently because of the accumulation of APP CTFs.

PDEs play a central role in signal transduction by regulating intracellular levels of cAMP and cyclic GMP (García-Osta et al., 2012; Houslay and Milligan, 1997; Peng et al., 2014). PDE isoenzymes are classified into 11 families (PDE1–PDE11). Apart from PDE8B, PDE1B was also detected in this experiment. PDE1B from CHO cells expressing C83 showed 0.8-fold expression and that from CHO cells expressing C89 showed 1.1-fold expression (Supplementary Excel File), suggesting that the levels of PDE1B did not change. Other PDEs were not detected.

In the brain, PDE1, PDE2, PDE3, PDE4, PDE5A, PDE7A, PDE7B, PDE8B, PDE9A, PDE10A, and PDE11A were expressed. As these enzymes control the levels of cAMP and/or cyclic GMP in cells that are crucial for neural function, PDE inhibitors represent promising candidate drugs for the treatment of altered cognition states (García-Osta et al., 2012). The effectiveness of repeated administration of PDE3 inhibitor (cilostazol), PDE4 inhibitor (rolipram or GEBR-7b), PDE5 inhibitor (sildenafil or tadalafil), PDE7 inhibitor (S14), and PDE9A inhibitor (BAY 73–6691) has been demonstrated in several model animals of AD (Bruno et al., 2011; Cheng et al., 2010; García-Barroso et al., 2013; Gong et al., 2004; Kroker et al., 2014; Li et al., 2011; Peng et al., 2014; Perez-Gonzalez et al., 2013; Sierksma et al., 2013, 2014).

Because the increase of PDE8B may induce the hydrolysis of cAMP, our results suggest that APP-CTF accumulation triggers the hydrolysis of cAMP and subsequent cAMP/PKA/CREB pathway

impairment without Aβ involvement. It has already been reported that PDE8B is the only isozyme showing a significant increase in cortical areas and parts of the hippocampal formation of AD patients (Pérez-Torres et al., 2003). Furthermore, in the AD brain and some mouse models of AD, CREB activity is impaired (Gong et al., 2004).

Impairment of the cAMP/PKA/CREB pathway in AD has mainly been attributed to Aβ toxicity (Tong et al., 2001). However, our results indicate the possibility that APP-CTF accumulation, apart from Aβ, induces cAMP/PKA/CREB pathway impairment via an increase in the level of PDE. In addition, our preliminary result that the levels of cAMP were reduced in APP-CTF–accumulated PC12D and CHO cells (Supplementary Fig. 4) supports this possibility.

Furthermore, accumulations of APP CTFs may be common phenomena in AD. Presenilin mutations, which are known as major FAD mutations, cause a partial loss of γ-secretase cleavage function at ε-sites of APP and induce APP-CTF accumulation (Kametani, 2008; Robakis and Georgakopoulos, 2013). The Swedish mutation of APP increases β-site cleavage by BACE1 and increases the production of CTF C99, which is an insufficient substrate for γ-secretase ε-site cleavage (Funamoto et al., 2013). APP mutations near the γ-cleavage site also decrease the production of AICD (Wiley et al., 2005), suggesting that ε-site cleavage impairment and accumulation of APP cytoplasmic domain occur. In APP duplication, FAD and Down syndrome, generation of APP CTFs increase. Furthermore, in sporadic AD, APP-CTF C99 increases via BACE1 increase or BACE1 activity increases.

APP-CTF accumulation may induce an increase in the level of PDE, following cAMP reduction independent of Aβ involvement in AD. As for the precise molecular mechanism by which APP-CTF accumulation induces an increase in the level of PDE8B, further studies are required.

Disclosure statement

The authors have no conflicts of interests to report.

Acknowledgements

This work was supported by JSPS KAKENHI grant number 23390093 (Fuyuki Kametani).

Appendix A. Supplementary data

Supplementary data associated with this article can be found, in the online version, at http://dx.doi.org/10.1016/j.neurobiolaging.2014.09.029.

References

Asai, M., Yagishita, S., Iwata, N., Saido, T.C., Ishiura, S., Maruyama, K., 2011. An alternative metabolic pathway of amyloid precursor protein C-terminal fragments via cathepsin B in a human neuroglioma model. FASEB J. 25, 3720–3730.

Bruno, O., Fedele, E., Prickaerts, J., Parker, L.A., Canepa, E., Brullo, C., Cavallero, A., Gardella, E., Balbi, A., Domenicotti, C., Bollen, E., Gijselaers, H.J., Vanmierlo, T., Erb, K., Limebeer, C.L., Argellati, F., Marinari, U.M., Pronzato, M.A., Ricciarelli, R., 2011. GEBR-7b, a novel PDE4D selective inhibitor that improves memory in rodents at non-emetic doses. Br. J. Pharmacol. 164, 2054–2063.

Chen, A.C., Selkoe, D.J., 2007. Response to: Pardossi-Piquard et al., "Presenilin-dependent transcriptional control of the Aβ-degrading enzyme neprilysin by intracellular domains of betaAPP and APLP." Neuron 46, 541-554. Neuron 53, 479–483.

Cheng, Y.F., Wang, C., Lin, H.B., Li, Y.F., Huang, Y., Xu, J.P., Zhang, H.T., 2010. Inhibition of phosphodiesterase-4 reverses memory deficits produced by Abeta25–35 or Abeta1–40 peptide in rats. Psychopharmacology (Berl) 212, 181–191.

Cupers, P., Orlans, I., Craessaerts, K., Annaert, W., De Strooper, B., 2001. The amyloid precursor protein (APP)-cytoplasmic fragment generated by gamma-secretase is rapidly degraded but distributes partially in a nuclear fraction of neurones in culture. J. Neurochem. 78, 1168–1178.

Edison, P., Archer, H.A., Hinz, R., Hammers, A., Pavese, N., Tai, Y.F., Hotton, G., Cutler, D., Fox, N., Kennedy, A., Rossor, M., Brooks, D.J., 2007. Amyloid, hypometabolism, and cognition in Alzheimer disease: an [11C]PIB and [18F]FDG PET study. Neurology 68, 501–508.

Funamoto, S., Sasaki, T., Ishihara, S., Nobuhara, M., Nakano, M., Watanabe-Takahashi, M., Saito, T., Kakuda, N., Miyasaka, T., Nishikawa, K., Saido, T.C., Ihara, Y., 2013. Substrate ectodomain is critical for substrate preference and inhibition of gamma-secretase. Nat. Commun. 4, 2529.

García-Barroso, C., Ricobaraza, A., Pascual-Lucas, M., Unceta, N., Rico, A.J., Goicolea, M.A., Sallés, J., Lanciego, J.L., Oyarzabal, J., Franco, R., Cuadrado-Tejedor, M., García-Osta, A., 2013. Tadalafil crosses the blood–brain barrier and reverses cognitive dysfunction in a mouse model of AD. Neuropharmacology 64, 114–123.

García-Osta, A., Cuadrado-Tejedor, M., García-Barroso, C., Oyarzábal, J., Franco, R., 2012. Phosphodiesterases as therapeutic targets for Alzheimer's disease. ACS Chem. Neurosci. 3, 832–844.

Giacobini, E., Gold, G., 2013. Alzheimer disease therapy—moving from amyloid-β to tau. Nat. Rev. Neurol. 9, 677–686.

Gong, B., Vitolo, O.V., Trinchese, F., Liu, S., Shelanski, M., Arancio, O., 2004. Persistent improvement in synaptic and cognitive functions in an Alzheimer mouse model after rolipram treatment. J. Clin. Invest. 114, 1624–1634.

Houslay, M.D., Milligan, G., 1997. Tailoring cAMP-signalling responses through isoform multiplicity. Trends Biochem. Sci. 22, 217–224.

Jiang, Y., Mullaney, K.A., Peterhoff, C.M., Che, S., Schmidt, S.D., Boyer-Boiteau, A., Ginsberg, S.D., Cataldo, A.M., Mathews, P.M., Nixon, R.A., 2010. Alzheimer's-related endosome dysfunction in Down syndrome is Abeta-independent but requires APP and is reversed by BACE-1 inhibition. Proc. Natl. Acad. Sci. U. S. A 107, 1630–1635.

Kametani, F., 2008. Epsilon-secretase: reduction of amyloid precursor protein epsilon-site cleavage in Alzheimer's disease. Curr. Alzheimer Res. 5, 165–171.

Kim, H.S., Kim, E.M., Lee, J.P., Park, C.H., Kim, S., Seo, J.H., Chang, K.A., Yu, E., Jeong, S.J., Chong, Y.H., Suh, Y.H., 2003. C-terminal fragments of amyloid precursor protein exert neurotoxicity by inducing glycogen synthase kinase-3β expression. FASEB J. 17, 1951–1953.

Kopan, R., Ilagan, M.X.G., 2004. Gamma-secretase: proteasome of membrane? Nat. Rev. Mol. Cell Biol. 5, 499–504.

Kroker, K.S., Mathis, C., Marti, A., Cassel, J.C., Rosenbrock, H., Dorner-Ciossek, C., 2014. PDE9A inhibition rescues amyloid beta-induced deficits in synaptic plasticity and cognition. Neurobiol. Aging 35, 2072–2078.

Lauritzen, I., Pardossi-Piquard, R., Bauer, C., Brigham, E., Abraham, J.D., Ranaldi, S., Fraser, P., St-George-Hyslop, P., Le Thuc, O., Espin, V., Chami, L., Dunys, J., Checler, F., 2012. The β-secretase-derived C-terminal fragment of betaAPP, C99, but not Abeta, is a key contributor to early intraneuronal lesions in triple-transgenic mouse hippocampus. J. Neurosci. 32, 16243–16255.

Li, Y.F., Cheng, Y.F., Huang, Y., Conti, M., Wilson, S.P., O'Donnell, J.M., Zhang, H.T., 2011. Phosphodiesterase-4D knock-out and RNA interference-mediated knock-down enhance memory and increase hippocampal neurogenesis via increased cAMP signaling. J. Neurosci. 31, 172–183.

Li, Y., Rinne, J., Mosconi, L., Pirraglia, E., Rusinek, H., DeSanti, S., Kemppainen, N., Någren, K., Kim, B.C., Tsui, W., Leon, M., 2008. Regional analysis of FDG and PIB-PET images in normal aging, mild cognitive impairment, and Alzheimer's disease. Eur. J. Nucl. Med. Mol. Imaging 35, 2169–2181.

Marambaud, P., Wen, P.H., Dutt, A., Shioi, J., Takashima, A., Siman, R., Robakis, N.K., 2003. A CBP binding transcriptional repressor produced by the PS1/epsilon-cleavage of N-cadherin is inhibited by PS1 FAD mutations. Cell 114, 635–645.

Ohkawara, T., Nagase, H., Koh, C.S., Nakayama, K., 2011. The amyloid precursor protein intracellular domain alters gene expression and induces neuron-specific apoptosis. Gene 475, 1–9.

Oster-Granite, M.L., McPhie, D.L., Greenan, J., Neve, R.L., 1996. Age-dependent neuronal and synaptic degeneration in mice transgenic for the C terminus of the amyloid precursor protein. J. Neurosci. 16, 6732–6741.

Pardossi-Piquard, R., Dunys, J., Kawarai, T., Sunyach, C., Alves da Costa, C., Vincent, B., Sevalle, J., Pimplikar, S., St George-Hyslop, P., Checler, F., 2007. Response to correspondence: Pardossi-Piquard et al., "Presenilin-dependent transcriptional control of the Aβ-degrading enzyme neprilysin by intracellular domains of βAPP and APLP." Neuron 46, 541-554. Neuron 53, 483–486.

Pardossi-Piquard, R., Petit, A., Kawarai, T., Sunyach, C., Alves da Costa, C., Vincent, B., Ring, S., D'Adamio, L., Shen, J., Muller, U., 2005. Presenilin-dependent transcriptional control of the Aβ-degrading enzyme neprilysin by intracellular domains of βAPP and APLP. Neuron 46, 541–554.

Passer, B., Pellegrini, L., Russo, C., Siegel, R.M., Lenardo, M.J., Schettini, G., Bachmann, M., Tabaton, M., D'Adamio, L., 2000. Generation of an apoptotic intracellular peptide by gamma-secretase cleavage of Alzheimer's amyloid â protein precursor. J. Alzheimers Dis. 2, 289–301.

Peng, S., Sun, H., Zhang, X., Liu, G., Wang, G., 2014. Effects of selective phosphodiesterases-4 inhibitors on learning and memory: a review of recent research. Cell Biochem. Biophys. 70, 83–85.

Pera, M., Alcolea, D., Sánchez-Valle, R., Guardia-Laguarta, C., Colom-Cadena, M., Badiola, N., Suárez-Calvet, M., Lladó, A., Barrera-Ocampo, A., Sepulveda-Falla, D., Blesa, R., Molinuevo, J., Clarimón, J., Ferrer, I., Gelpi, E., Lleó, A., 2013. Distinct patterns of APP processing in the CNS in autosomal-dominant and sporadic Alzheimer disease. Acta Neuropathol. 125, 201–213.

Perez-Gonzalez, R., Pascual, C., Antequera, D., Bolos, M., Redondo, M., Perez, D.I., Pérez-Grijalba, V., Krzyzanowska, A., Sarasa, M., Gil, C., Ferrer, I., Martinez, A., Carro, E., 2013. Phosphodiesterase 7 inhibitor reduced cognitive impairment and pathological hallmarks in a mouse model of Alzheimer's disease. Neurobiol. Aging 34, 2133–2145.

Pérez-Torres, S., Cortés, R., Tolnay, M., Probst, A., Palacios, J.M., Mengod, G., 2003. Alterations on phosphodiesterase type 7 and 8 isozyme mRNA expression in Alzheimer's disease brains examined by in situ hybridization. Exp. Neurol. 182, 322–334.

Robakis, N.K., 2011. Mechanisms of AD neurodegeneration may be independent of Abeta and its derivatives. Neurobiol. Aging 32, 372–379.

Robakis, N.K., Georgakopoulos, A., 2014. Allelic interference: a mechanism for trans-dominant transmission of loss of function in the neurodegeneration of familial Alzheimer's disease. Neurodegener. Dis. 13, 126–130.

Sierksma, A.S., Rutten, K., Sydlik, S., Rostamian, S., Steinbusch, H.W., van den Hove, D.L., Prickaerts, J., 2013. Chronic phosphodiesterase type 2 inhibition improves memory in the APPswe/PS1dE9 mouse model of Alzheimer's disease. Neuropharmacology 64, 124–136.

Sierksma, A.S., van den Hove, D.L., Pfau, F., Philippens, M., Bruno, O., Fedele, E., Ricciarelli, R., Steinbusch, H.W., Vanmierlo, T., Prickaerts, J., 2014. Improvement of spatial memory function in APPswe/PS1dE9 mice after chronic inhibition of phosphodiesterase type 4D. Neuropharmacology 77, 120–130.

Tong, L., Thornton, P.L., Balazs, R., Cotman, C.W., 2001. Beta-amyloid-(1–42) impairs activity-dependent cAMP-response element-binding protein signaling in neurons at concentrations in which cell survival is not compromised. J. Biol. Chem. 276, 17301–17306.

Wiley, J.C., Hudson, M., Kanning, K.C., Schecterson, L.C., Bothwell, M., 2005. Familial Alzheimer's disease mutations inhibit gamma-secretase-mediated liberation of beta-amyloid precursor protein carboxy-terminal fragment. J. Neurochem. 94, 1189–1201.

ACTA NEUROPATHOLOGICA COMMUNICATIONS

RESEARCH Open Access

Tau accumulation in the nucleus accumbens in tangle-predominant dementia

Ito Kawakami[1,2], Masato Hasegawa[3], Tetsuaki Arai[1,4], Kenji Ikeda[1,5], Kenichi Oshima[6], Kazuhiro Niizato[6], Naoya Aoki[1,2], Katsuse Omi[2], Shinji Higashi[1], Masato Hosokawa[1], Yoshio Hirayasu[2] and Haruhiko Akiyama[1*]

Abstract

Background: Tangle-predominant dementia (TPD) is characterized neuropathologically by numerous neurofibrillary tangles in the limbic areas with no or occasional senile plaques throughout the brain. TPD is an under-recognized disease, while it is a common cause of dementia in those over 80 years of age. In the present study, we describe hyperphosphorylated tau (tau) accumulation in the nucleus accumbens (Acb) in patients with TPD.

Results: We investigated immunohistochemically the brain tissues from 7 patients with TPD, 22 with Alzheimer disease (AD) and 11 non-demented aged subjects. In the Acb of all 7 TPD patients, a considerable number of tau positive neurons were found together with many neuropil threads. The tau deposits in the Acb were labeled with all the anti-tau antibodies used in the present study. They included conformational change-specific, phosphorylation-specific and phosphorylation-independent antibodies. The Acb consists of the predominant medium-sized neurons with a small number of large neurons. Both the cell types were affected by tau pathology in TPD. Tau accumulation in the majority of such neurons appeared to be pretangle-like, diffuse deposits with only occasional paired helical filament formation. Tau positive neurons were also found in the Acb in some AD and non-demented aged subjects but much fewer in the majority of cases. The immunoblot analyses of fresh frozen samples of the Acb and parahippocampal cortex from 3 TPD and 3 AD patients revealed that the insoluble tau in the Acb was a mixture of the 3- and 4-repeat isoforms.

Conclusions: To our knowledge, this is the first report on the occurrence of tau accumulation in the Acb in TPD. The Acb receives direct and massive projections from the hippocampal CA1 and subiculum where neurofibrillary tangles are known to occur more frequently in TPD than in AD. The prevalence of abnormal tau accumulation in the Acb in TPD may support the idea that abnormal tau aggregation propagates via neural circuits. In all but one TPD cases used in this study, delusion was a consistent clinical feature. Whether the Acb tau accumulation is related to the psychiatric symptoms in TPD may be an issue for further investigation.

Keywords: Neurofibrillary tangle, Alzheimer disease, Propagation, Delusion

Introduction

Tangle-predominant dementia (TPD), which is also referred to as neurofibrillary tangle predominant dementia, limbic neurofibrillary tangle dementia or senile dementia of the neurofibrillary tangle type, is a poorly understood and under-recognized tauopathy. TPD has been reported to comprise 0.7 to 5.8% of elderly patients with dementia [1-3]. TPD is characterized neuropathologically by numerous neurofibrillary tangles (NFT) in the limbic areas with no or occasional senile plaques throughout the brain. The clinical features of TPD include the late-adult onset, which is over 80 years in the majority of cases, and slow progression of dementia as compared with Alzheimer's disease (AD). In patients with TPD, there is a propensity for the memory disturbance to be conspicuous with relative preservation of other cognitive functions. However, it is hard to distinguish TPD from AD on a clinical basis and, thus, diagnosis of TPD in most cases is only made postmortem.

The etiology of TPD is unknown. NFT in TPD consist of both 3-repeat (3R) and 4-repeat (4R) isoforms of hyperphosphorylated tau (tau), and the neuronal cell types

* Correspondence: akiyama-hr@igakuken.or.jp
[1]Dementia Research Project, Tokyo Metropolitan Institute of Medical Science, 2-1-6 Kamikitazawa, Setagaya-ku, Tokyo 156-8506, Japan
Full list of author information is available at the end of the article

bearing NFT in TPD are similar to those in AD. TPD seems to be a disorder that is related to AD, if it is not an atypical form of AD. TPD, as a subtype of tauopathy, is also included in the group described as neuropathologically-defined frontotemporal lobar degeneration [4,5]. In fact, cortical lesions in TPD are localized to the mediobasal temporal cortex. Thus, the situation of TPD in the groups of dementing neurodegenerative diseases remains unclear from both clinical and neuropathological points of view.

A neuropathological characteristic of TPD is the heavy accumulation of NFT in the hippocampal regions, with few or occasional NFT in neocortical areas beyond the collateral sulcus. Compared with AD patients in which a similar number of NFT occurs in the hippocampal regions, neuronal cell loss, tissue rarefaction and gliosis are less prominent in TPD, even in NFT rich areas. Changes in the neocortex are modest, with well-preserved laminar structures and unremarkable neuronal cell loss. The cortical expansion of NFT in TPD is considered to follow in principle the hierarchical pathway described in AD by Braak and Braak [6] but to be limited to stage IV. In the hippocampal regions, the density of NFT is higher than in AD [7] and ghost tangles are very frequent [3]. Tau pathology in the subcortical structures in TPD has not been well studied. The occurrence of NFT in the amygdala, the nucleus basalis of Meynert, the substantia nigra and the locus coeruleus, regions where NFT frequently occur in AD cases, have been reported in TPD [3,8].

The nucleus accumbens (Acb) is located in the region where the caudate head and the rostral putamen meet near the septum pellucidum (Figure 1). The Acb and the olfactory tubercle form the ventral striatum in the forebrain. The Acb is a key component of the limbic striatal loop in which the Acb receives fibers from the prefrontal cortex, amygdala, hippocampus and ventral tegmental area (VTA) and projects to the ventral pallidum [9-12]. The ventral pallidum sends axonal projections to the dorsomedial thalamic nucleus, which then projects to the prefrontal cortex to close the loop [13,14]. The dopaminergic input from the VTA modulate the activity of this loop [15]. The Acb is considered to be involved in cognition, emotion and emotional behaviors such as pleasure, fear, aggression, addiction and reward [16,17]. The limbic striatal loop is, therefore, one of the major targets of studies on the pharmacological actions of anti-psychotic drugs [18,19].

In the present study, we found the frequent and consistent tau accumulation in the Acb in TPD. Tau positive neurons were also found in the Acb in some AD and on-demented aged subjects but much fewer in the majority of such cases. We speculate that the lesions in the Acb play a role in some psychiatric symptoms such as delusion, which is often conspicuous in TPD.

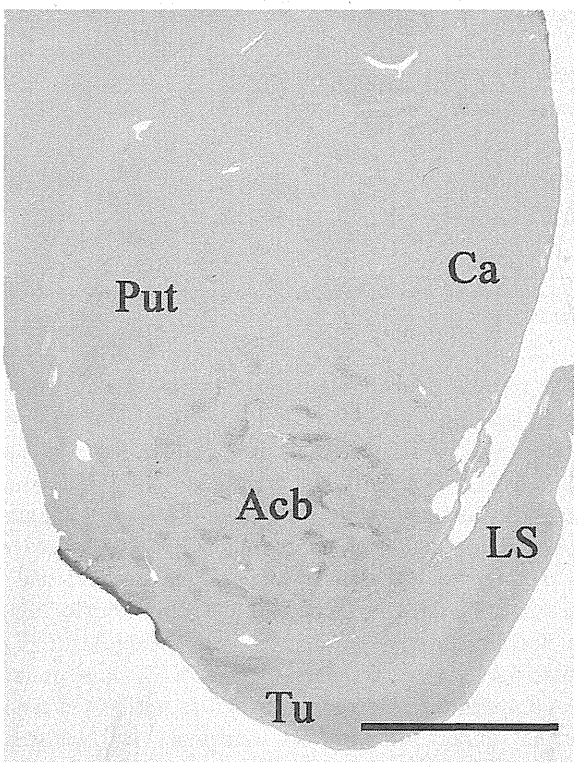

Figure 1 A semi-macro photograph of the basal ganglia from a TPD case stained with AT8. Faint immunoreaction is seen in the nucleus accumbens (Acb), lateral septal nucleus (LS) and the olfactory tubercle (Tu) even at this low power magnification. Ca: caudate nucleus; Put: putamen. Scale bar = 1 cm.

Materials and methods

We used brain tissues, archived in our laboratory, from 7 patients with TPD, 22 with AD and 11 subjects without dementia or other neurological disease. The demography, Braak and Braak's NFT stages and brain weight in each patient group are summarized in Table 1. Diagnoses were initially made on a clinical basis and were confirmed in every case by neuropathological examination. Clinical and neuropathological diagnoses of TPD followed the descriptions in previous articles [3,7,20]. Diagnoses of AD were made if the CERAD plaque score was 'C' [21] and the Braak and Braak's NFT stage was IV or higher [6]. In TPD and AD cases with the NFT stage III or IV, Lewy body pathology was confirmed to be absent or mild/stage 1 [22] in the hippocampus, parahippocampal gyrus and temporal neocortex to exclude the possibility of Dementia with Lewy bodies. In all cases, the patient or, in any case where the patient had died, his/her next of kin gave the written consent for autopsy and postmortem analyses for research purposes. This study was approved by the ethics committee in the Tokyo Metropolitan Institute of Medical Science and was performed in accordance with the ethical standards laid down in the 1964 declaration of Helsinki and its later amendments.

Table 1 Summary of patient groups used in this study

	TPD		AD		Non-demented
Braaks' NFT stages	**III or IV**	**IV**	**V**	**VI**	**I-III**
Number of cases	7	10	8	4	11
Gender (male/female)	1/6	6/4	4/4	2/2	7/4
Age at death*	88.4 ± 7.2	81.5 ± 8.5	86 ± 3.5	81.5 ± 8.8	81 ± 7.0
Disease duration (y)*	4.7 ± 2.9	6.1 ± 6.7	6.2 ± 3.5	6.6 ± 6.0	n/a
Brain weight (g)*	1,137 ± 135.3	1,134 ± 174.8	1,119 ± 77.2	1,008 ± 156.5	1,146 ± 77.1

TPD, Tangle-predominant dementia; *AD*, Alzheimer's disease; *NFT*, neurofibrillary tangles.
*Data are shown as mean ± S.D.

For routine neuropathological examinations, formalin-fixed, paraffin-embedded brain blocks were cut into 10 μm thick sections and stained with hematoxylin and eosin (HE), Klüver-Barrera, modified Gallyas-Braak and methenamine silver staining. Tissue sections of the mediobasal temporal cortex containing the hippocampus, entorhinal cortex and temporal neocortex were stained for tau and amyloid β protein (Aβ) by immunohistochemistry. Sections of the rostral striatum with the Acb and the septal nuclei were stained for tau. In TPD cases, additional tau immunohistochemistry was performed for the nucleus basalis of Meynert, amygdala and substantia nigra. The hippocampus, parahippocampal gyrus and adjacent temporal neocortex were also stained for phosphorylated α-synuclein and phosphorylated TDP-43 in TPD cases.

For more detailed immunohistochemical analyses, small blocks of brain the tissues were dissected at autopsy and fixed in 4% paraformaldehyde (PFA) for 2 days. The cryocut sections of 30 μm thickness were used for the high sensitive, free-floating immunhistochemical staining [23]. The antibodies used in this study are listed in Additional file 1: Table S1. The primary antibody labeling was visualized with 3,3′-diaminobenzidine as a chromogen, in combination with the Envision Plus® kit (Dako Japan, Tokyo). For enhanced thioflavin-S staining, tissue sections were pretreated with $KMnO_4$ for 20 min and, subsequently, with sodium borohydride for 4 min [24]. Sections were then stained with 0.05% thioflavin-S in 50% ethanol in the dark for 8 min, followed by differentiation in two changes of 80% ethanol for 10 sec each time and three washes in large volumes of distilled water. Following incubation in a high salt solution containing 411 mM NaCl, 8.1 mM KCl, 30 mM Na_2HPO_4 and 5.2 mM KH_2PO_4, pH 7.2 at 4°C for 30 min, sections were briefly rinsed with distilled water and observed by fluorescence microscopy.

For immunoelectron microscopy, both post-embedded and pre-embedded procedures were used. For the former, the 4% PFA-fixed small tissues were embedded in LR White Resin® (London Resin, U.K.) without further fixation. The ultra-thin sections were stained with AT8, which was followed by incubation with anti-mouse IgG conjugated with 10 or 20 nm gold colloidal particles (BBinternational, U.K.). For the pre-embedding procedure, the 4% PFA-fixed free-floating sections were stained with AT8 in combination with Alexa Fluor 488 FluoroNanogold anti-mouse IgG (Nanoprobes, U.S.A.). Following examination by fluorescence microscopy to localize the positive labeling, the sections were postfixed with 2% glutaraldehyde and then treated with HQ Silver Enhancement Kit (Nanoprobes, U.S.A.). After the treatment with 1% osmium tetroxide, which was followed by 2% uranyl acetate, the sections were embedded in epoxy resin (Querol 812, Nissin EM, Japan). Ultrathin sections were cut and observed by a transmission electron microscope (JEM-1400, JEOL, Japan).

For immunoblot analyses, fresh frozen samples of the Acb and the parahippocampal cortex were obtained from 3 TPD cases (cases 3, 4 and 6) and 3 AD cases. The Braak and Braak's NFT stages of the AD cases were 4, 5 and 6, respectively. Brain tissue was homogenized in 2 vol of TS buffer (50 mM Tris–HCl, 150 mM NaCl, pH 7.5), with a mixture of protease inhibitors and centrifuged at 200,000 g for 20 minutes at 4°C. The supernatant was taken as the soluble fraction and the pellet was used to further extract the sarkosyl-insoluble fraction as described previously [25]. Dephosphorylation of the sarkosyl-insoluble fractions was performed by incubation of the samples with Escherichia coli alkaline phosphatase (type III, Sigma) as described previously [25]. HT7, a pan-tau monoclonal antibody (Additional file 1: Table S1), was used for immunoblotting. Primary antibody labeling on the membranes was visualized with 3,3′-diaminobenzidine as a chromogen, in combination with a Vectastain ABC kit® (Vector Lab., USA).

For semiquantitative analyses of immunohistochemically stained tissue sections, the density of AT8 positive tau accumulation was graded to be 0 for absent, 1 for low, 2 for intermediate and 3 for high, based on microscopic observations at ×200 magnification. The Acb, septal nuclei, caudate nucleus, hippocampal CA1, entorhinal cortex and temporal neocortex were assessed in TPD, AD and non-demented aged subjects. The Mann–Whitney *U* test was used for statistical analyses using Graph Pad Prism 4 software (Graph Pad Software, U.S.A.).

Results

TPD cases used in the present study

The demographic, pathologic, and clinical information of the TPD cases used in the present study is summarized in Tables 1 and 2. In general, both the clinical and neuropathological features are similar to those described in previous reports [1-3,7,26,27]. The average age at death is higher than that in AD. Moderate dementia was noted in 5 of the 7 cases but the other two were diagnosed as having mild cognitive impairment. Delusion was evident in 6 cases. Brain atrophy was mild, if present, and senile plaques were either absent or rare. Lacunar infarcts were seen in the globus pallidus in 2 cases. In all cases, heavy tau accumulation was seen in the limbic regions in the forms of NFT, diffuse cytoplasmic accumulations and neuropil threads. Tau accumulation was heavier in the subiculum and the CA1 region than in the entorhinal and transentorhinal cortices. Tau was also deposited in the amygdala, the septal nuclei and the basal nucleus of Meynert, and, less frequently, in the caudate nucleus and substantia nigra. A small amount of tau was found in the temporal neocortex but only in 3 cases. Such limbic-predominant distribution of tau pathology is consistent with previous reports [1,2,26,28]. A small number of argyrophilic grains were present in 2 cases.

Tau accumulation in the Acb in TPD

In addition to the previously reported tau distribution, we found a considerable number of tau positive neurons in the Acb in all TPD cases used in this study (Figures 1 and 2). Similarly to the hippocampus, numerous neuropil threads were associated with tau positive neurons (Figure 2A). The tau positive neurons and neuropil threads were labeled with all the anti-tau antibodies used in the present study (Figures 2A-D). They included conformational change-specific, phosphorylation-specific and phosphorylation-independent antibodies (Additional file 1: Table S1). The staining pattern varied, which partly depends on the affinity of the antibody and the localization of the antigen epitope recognized by each antibody. Preservation of the epitope in tissue sections is affected by aggregation, degradation and post-mortem processing such as fixation. The majority of tau positive neurons in the Acb showed pretangle-like, diffuse or granular accumulation of tau in the cytoplasm (Figures 2B). Flame-like NFT, the common form in the hippocampus in TPD, were also present but not frequent (Figure 2B, arrow). The vast majority of tau positive neurons were medium sized but, occasionally, large neurons were also stained positively for tau (Figure 2D, arrow). Tau positive neurons and threads were not distributed evenly in the Acb. Rather, areas with sparse- and dense-tau pathology were intermingled (Figure 2E).

Table 2 Demography and basic clinical and neuropathological features of TPD cases

	Case 1	Case 2	Case 3	Case 4	Case 5	Case 6	Case 7
Age at death	89	102	90	85	89	78	86
Sex	F	F	F	F	F	M	F
Dementia	+	+	+	+	MCI	MCI	+
Psychiatric symptoms							
Delusion	+	+	+	+	+	+	-
Anxiety	+	-	-	-	-	-	-
Depression	-	-	-	+	-	-	-
Brain weight (g)	940	970	1170	1300	1230	1220	1130
Atrophy	mi(Fr)	mi(Fr/T)	-	-	-	-	-
Plaque stage (1)	0	0	A*	0	0	0	0
NFT stage (1)	III	III	III	III	IV	III	III
Argyrophilic grain stage (2)	0	0	0	0	II	II	0
Hippocampal sclerosis	-	-	+	-	-	-	-
Vascular lesions	+	-	-	+	-	-	-
α-synuclein (hip/T**)	+§	-	-	-	-	-	-
TDP-43 (hip/T**)	-	-	-	-	-	-	-
Acb tau score	3	2	2	3	3	2	3

F, Female; *M*, Male; *MCI*, Mild cognitive impairment; *mi*, Mild; *Fr*, Frontal; *T*, Temporal; *Acb*, The nucleus accumbens. *A small number of diffuse Aβ deposits were seen in the temporal cortex. The Acb tau score was determined according to the method described in the text. (1) The senile plaque and NFT staging were based on the description by Braak and Braak [6]. (2) The argyrophilic grain staging was based on the description by Saito et al. [29]. **Immunohistochemistry for α-synuclein and TDP-43 was performed in tissue sections of the hippocampus, parahippocampal gyrus and adjacent temporal neocortex. § α-Synuclein pathology in this case was mild, corresponding to stage 1 by the 3rd report of the DLB consortium [22].

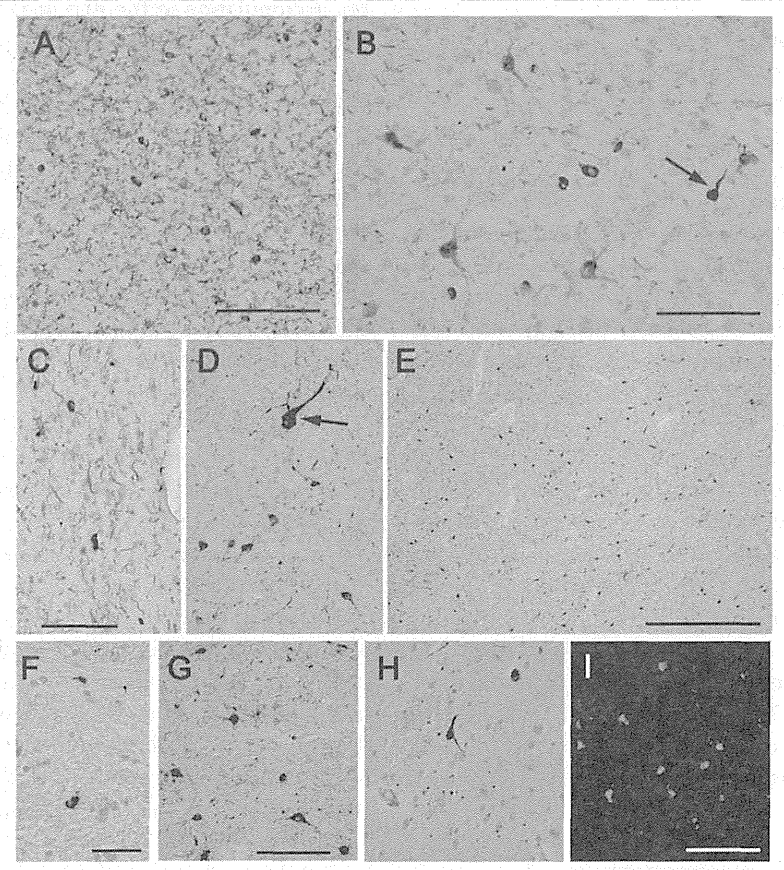

Figure 2 Tau accumulation in the Acb in TPD. A through **G** are immunohistochemistry with phosphorylation or conformational change specific tau antibodies. **A**, **B**, **C** and **I**: 4% paraformaldehyde-fixed, frozen-cut, 30 μm thick Sections. **D** through **H** are formalin-fixed, 10 μm thick, paraffin Sections. **A**: immunohistochemistry with AP422. Tau positive neurons are associated with many neuropil threads. Scale bars = 200 μm. **B**: immunohistochemistry with PHF-1. The majority of tau positive neurons show pretangle-like, diffuse or granular cytoplasmic labeling. Among them, apparent NFT are also seen but less frequently (arrow). Scale bar = 100 μm. **C**: immunohistochemistry with MC1, a conformational change specific antibody. Scale bar = 100 μm. **D** through **G** are immunohistochemistry with AT8. **D**: the vast majority of tau positive neurons are of medium-size but, occasionally, large neurons are also stained positively for tau (arrow). At the same magnification as **C. E**: tau positive neurons are not evenly distributed in the Acb. Scale bar = 500 μm. **F**: a glial coiled body. Scale bar = 25 μm. **G** and **H**: the nearby sections from the same case with AT8 immunohistochemistry **(G)** and Gallyas-Braak staining **(H)**. **I**: thioflavin S staining reveals granular cytoplasmic labeling of neurons. Scale bar = 100 μm.

Occasional glial coiled bodies were seen in the majoriy, if not all, of the cases (Figure 2F). Occurrence of glial coiled bodies in other brain regions in TPD has been reported previously [3]. Gallyas-Braak staining labeled only a small number of NFT in the Acb, while tau immunohistochemistry of nearby sections from the same patient revealed many positive cells (Figure 2G and 2H). Enhanced thioflavin-S staining labeled many neurons (Figure 2I).

The density of tau positive neurons and neuropil threads varied somewhat among the TPD cases. In TPD, no clear association was seen between the degree of Acb tau pathology and the Braak and Braak's NFT stage or the presence or absence of Aβ deposits, argyrophilic grains [29] and vascular lesions (Table 2). Despite the consistent tau accumulation in the Acb in TPD, we were not able to find severe neuronal loss or gliosis by HE staining.

Immunoelectron microscopy of the Acb in TPD with a tau antibody, AT8, revealed positive labeling of granular structures in the neurons (Figure 3A). Small and sparse bundles of short filamentous structures were occasionally seen to be stained positively for AT8 in the neuronal cytoplasm and neuropil (Figure 3B). Some of them showed morphology consistent with paired helical filaments (PHF). Thus, the ultrastructure of tau accumulation in the Acb was different from that in the hippocampal CA1 region, where dense and long bundles of PHF were frequent and intensely labeled for AT8 (Figure 3C).

Tau pathology in the Acb in AD and non-demented aged subjects

We then investigated the Acb in AD and non-demented, aged subjects. Tau positive neurons were found in some,

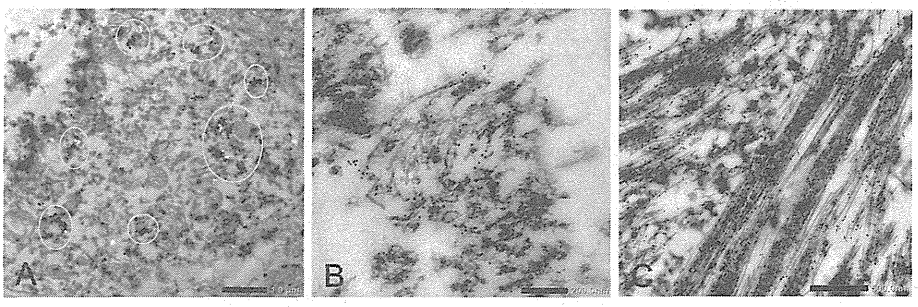

Figure 3 Immunoelectron microscopy of TPD brain with AT8 and immunogold labeling. A: in the Acb, the immunogold labeling in neurons was mostly localized to the granular structures (indicated by circles). Paired-helical filaments (PHF) were rare. Scale bar = 1.0 μm. **B**: sparse bundles of PHF were scattered in the neuronal cytoplasm. Scale bar = 200 nm. **C**: in the hippocampal CA1 region, prominent bundles of AT8 positive PHF were seen. Scale bar = 500 nm.

but not all, AD patients and non-demented, aged subjects (Additional file 2: Figure S1A). In these groups, however, only a limited number of cases showed tau pathology which was similarly abundant to that in TPD (Figure 4). In AD patients with heavy tau accumulation in the Acb, the caudate nucleus was also affected, a feature which distinguished AD from TPD. In TPD, the caudate tau lesions were either absent or, if present, very mild in all cases. In addition, senile plaques with tau positive dystrophic neurites were scattered in the Acb of such AD cases (Additional file 2: Figure S1B). In AD cases with mild tau pathology in the Acb, large neurons preferentially contained tau, a finding which was similar to the caudate nucleus in AD. In AD cases with heavy tau pathology in the Acb, such large neuron predominance became unclear and many tau positive, medium-sized neurons were seen. In both AD and non-demented, aged subjects, neuropil threads were also present in those with tau positive neurons in the Acb (Additional file 2: Figure S1C). The form of tau accumulation in AD patients and non-demented, aged subjects was similar to that in TPD, being predominantly pre-tangle like, diffuse accumulation in the cytoplasm.

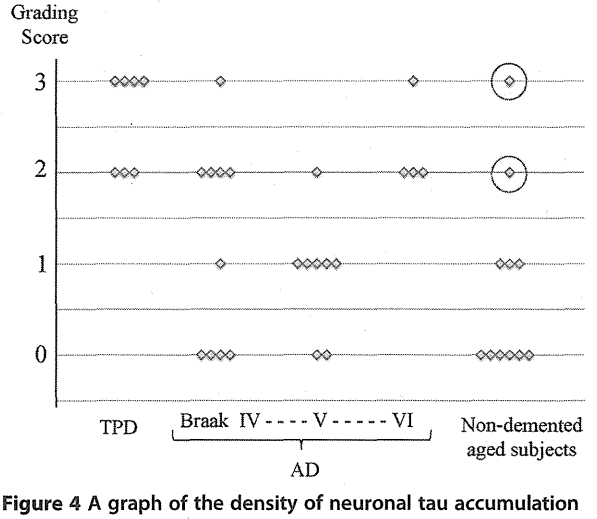

Figure 4 A graph of the density of neuronal tau accumulation in the Acb. The density of tau accumulation was graded as being 0 for absent, 1 for low, 2 for intermediate and 3 for high. Statistically significant differences were seen between TPD cases and non-demented, aged subjects ($P = 0.0031$) as well as AD cases in NFT stage IV ($P = 0.0192$) and V ($P = 0.0022$). The points encircled by a broken line in the non-demented, aged group indicate that the cases were over age 90.

The density of neuronal tau accumulation was graded to be 0 (absent) through 3(high) in AT8 immunostained tissue sections. Figure 4 illustrates the results in the Acb. Tau density in the Acb in the AD group was highly variable, except that the cases in Braak and Braak's NFT stage VI were either grade 2 or 3. Statistically significant differences were seen between the TPD cases and the non-demented, aged subjects ($P = 0.0031$) as well as the AD cases with NFT stage IV ($P = 0.0192$) and those with NFT stage V ($P = 0.0022$). Two non-demented, aged subjects with tau accumulation in the Acb were both over age 90. These 2 cases, similarly to TPD, lacked tau accumulation in the caudate nucleus and showed more NFT in the subiculum than in the entorhinal cortex. The results of semiquantitative analyses confirmed our observation that tau accumulation in the Acb was a remarkable finding in TPD. We performed similar analyses for a number of brain regions. The results are summarized in Table 3 as the averages of the graded scores for tau accumulation in each group. The concentration of tau pathology in the limbic structures, including the Acb and septal nuclei, in TPD contrasted with the broad distribution over the neocortex in AD.

Immunoblot analyses

The results of immunoblot analyses of samples from TPD and AD patients are shown in Figure 5. The tau band patterns in the sarkosyl insoluble fraction appeared to be essentially the same between TPD and AD, while the amount of insoluble tau was far smaller in the Acb than in the parahippocampal cortex in AD. It has to be noted that, because of the very high concentrations of insoluble tau in the parahippocampal cortex samples, the amounts of samples

Table 3 Summary of the semiquantitative grading of tau accumulation

	Braak stage	No. of cases	Acb	Caudate nucleus	Septal nucleus	CA1	Ent	Temp
TPD	III-IV	7	2.6	0.7	2.2	3	2.57	0.4
Non-demented	I-II	3	0	0	0	0.67	1	0
	III	8	1.13	0.25	0.63	1.38	2	1
AD	IV	10	1.2	0.6	1.4	2.67	3	1.4
	V	8	0.9	0.9	1.3	2.89	2.9	2.5
	VI	4	1.3	1.3	1.7	3	3	3

The numbers indicate averages of the scores in each group. The degree of tau pathology was qualitatively scored as 0: absent 1: low 2: intermediate 3: high. *TPD*, Tangle predominant dementia; *AD*, Alzheimer's disease; *NFT*, Neurofibrillary tangles; *Acb*, nucl. Accumbens; *CA1*, Hippocampal CA1 region; *Ent*, Entorhinal cortex; *Tmep*, Temporal neocortex.

applied to the gels had to be reduced in AD cases. This resulted in the relatively weak signals for the Acb samples in AD cases. The dephosphorylated samples of the Acb and parahippocampal cortex showed the 3R + 4R isoform pattern in both TPD and AD.

The Acb tau pathology and the presence/absence of clinical history of delusion

Finally, we examined if the degree of the Acb tau pathology was different between the subjects groups with and without the history of delusion in the clinical records (Additional file 3: Figure S2). In the group of subjects with Braaks' NFT stages III and IV, which included NFT stage III non-demented aged subjects, all TPD cases and NFT stage IV AD cases, the Acb tau score was higher in those with clinical history of delusion than those without it ($p = 0.033$). Similarly, the less conspicuous but still significant difference was seen in the group of all NFT stage AD cases ($p = 0.049$).

Discussions

There is significant overlap in the distribution of NFT between TPD and AD. However, an early genetic study of TPD cases indicated a paucity of the apolipoprotein E ε4 allele, which currently is the most powerful risk factor for AD [30]. More recently, a report has been made on the significant associations of TPD with the *MAPT* H1 haplotype as well as with some polymorphisms within the region of *MAPT* encoding the 3′ UTR [31]. Thus, together with the striking paucity of Aβ deposition, it seems that TPD is a unique neuropathological entity that has to be studied separately from AD.

The clinical and neuropathological features of the TPD patients we used in the present study generally agreed with those described in preceding articles [3,32]. In

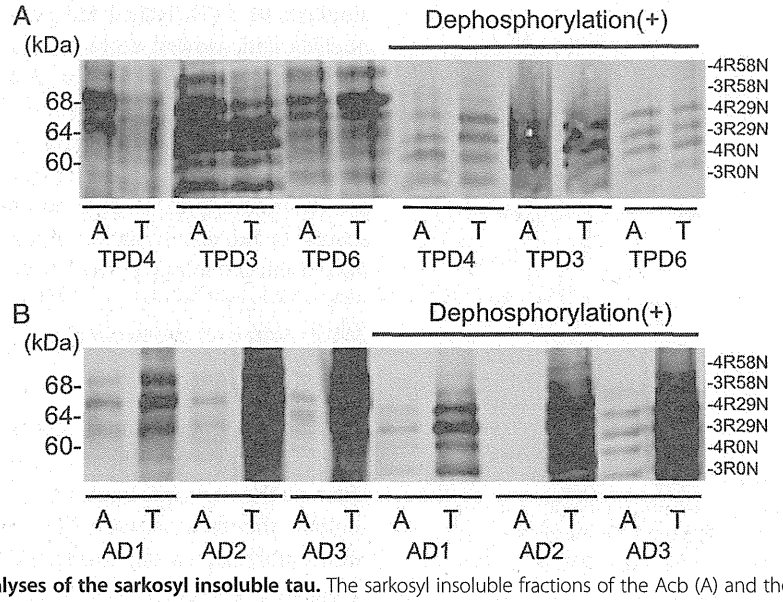

Figure 5 Immunoblot analyses of the sarkosyl insoluble tau. The sarkosyl insoluble fractions of the Acb (A) and the parahippocampal cortex (T) from TPD **(A)** and AD **(B)** were analyzed by immunoblot. A pan-tau antibody, HT7, was used. The Acb samples show the 3R + 4R isoform pattern similar to that in the parahippocampal cortices in both TPD and AD.

addition to the already well-known distribution of tau pathology, we found a considerable number of tau positive neurons and neuropil threads in the Acb. The Acb consists of the predominant medium-sized neurons and the occasional large neurons. Both cell types were affected by tau pathology in TPD. This contrasted AD with mild Acb tau pathology, in which large neurons were affected preferentially. Such a result is consistent with the previous reports which described that large neurons are more vulnerable in AD [33] and prone to tau accumulation [34]. In AD cases with the heavy Acb tau pathology, many medium-sized neurons were also tau positive. In the absence of TPD cases with the mild Acb tau pathology, it remains to be determined whether the difference is attributable to the distinct pathomechanisms between AD and TPD or to the variable vulnerability of different neuronal cell types.

The Acb may not be a region which is routinely sampled in a number of laboratories. Further, tau pathology in the Acb is not well stained by the Gallyas-Braak method. These facts together might explain the absence of previous reports on the occurrence of tau lesions in the Acb. The mechanism by which the Gallyas-Braak staining labels NFT remains to be determined. In TPD, insoluble tau consists of a mixture of the 3R and 4R isoforms in both the Acb and hippocampus, but NFT are intensely labeled by Gallyas-Braak staining in the latter. It may be noteworthy that, in the Acb, tau pathology occurs in a form of diffuse or granular cytoplasmic accumulations in the majority of tau positive neurons and that, ultrastructurally, PHF were rare. These contrasted with the hippocampal lesions where dense bundles of PHF were frequently seen. Obviously, factors that affect the reactivity of abnormal tau deposits to Gallyas-Braak staining need further clarification.

Tau pathology is considered to propagate in the brain from an affected region to another along the fiber connections, by spreading through the neuropil, or by both. A proposed mechanism for such propagation is a prion-like, seed-dependent conformational change and subsequent aggregation of the molecule, with a breakdown of the aggregate that generates the next seeds. In such a manner, the tau isoform pattern in the initial aggregates may be maintained in the later aggregate formations [35]. In the present study, we found that the Acb lesion in TPD was 3R + 4R tauopathy, a result which suggests the common origin of the tau pathology in the Acb with that in the hippocampus. The prevalence of diffuse cytoplasmic accumulations suggests that tau pathology in the Acb occurs later in the disease progression. In the hippocampus in TPD, many ghost tangles are seen, suggesting that the hippocampal lesions precede the Acb lesions.

Occurrence of NFT in the Acb in AD was reported previously [36,37]. In the present study, however, we have found that tau accumulation in TPD is more frequent and consistent than AD. The Acb receives direct and massive projections from the hippocampal CA1 and subiculum [14,38,39]. It has been repeatedly reported in TPD that the density of NFT is higher in the hippocampal CA1 and subiculum than in the entorhinal cortex [1,2,7,28]. Thus, the heavy tau pathology in the subiculum and CA1, through neural circuit-mediated propagation to the Acb, may result in the more pronounced tau accumulation in the Acb in TPD than in AD. Such an idea may be consistent with our finding that the difference in Acb tau pathology was statistically significant between TPD and AD in NFT stages IV and V but not in AD at stage VI. In AD with Acb lesions, tau accumulation was also found more frequently in the caudate nucleus than was the case in TPD. The caudate nucleus receives massive innervations from the cerebral cortex where, unlike TPD, tau pathology is severe in AD. On the other hand, the septal nuclei, like the Acb, receive direct projections from the subiculum and CA1 [14,38]. Again, we found, in the present study, heavier tau accumulation in these areas in TPD than in AD at NFT stages IV and V.

TPD is primarily an amnestic disease with relatively mild non-amnestic symptoms of dementia. In 6 of 7 TPD cases used in this study, however, delusion was a consistent clinical feature. This may be partly attributable to the fact that our brain tissue archive is principally based on the psychiatric hospital autopsies. However, occurrence of psychiatric symptoms has also been described in a number of previous reports on TPD. As an example, Jellinger et al. reported depression in 17.5% and paranoid ideas in 15% of TPD cases [3]. The Acb is part of the mesolimbic system in which the Acb receives dopaminergic input from the VTA. Recent evidence suggests that, in schizophrenia, functional abnormality in the Acb causes excessive release of dopamine from the VTA, which then results in the psychiatric symptoms [19,40-43]. While neuronal loss was not apparent in the Acb in TPD, it may be noteworthy that association of intraneuronal tau aggregation with clinical symptoms has been suggested in early stage AD lesions [44]. In AD, cases with more neocortical NFT were reported to be associated with more psychosis [45]. Thus, tau accumulation in the Acb could be related to the frequent delusion in TPD. Delusion and other psychotic symptoms may occur by multiple mechanisms in dementia patients. We have to note that 2 of the 7 TPD cases had argyrophilic grain pathology and that psychotic symptoms are known to be common in the patients with argyrophilic grain disease [46]. Whether the Acb tau accumulation is related to the psychiatric symptoms in TPD may be an issue for further investigation.

In the present study, we found that tau pathology occurred unevenly in the Acb in TPD (Figures 1 and 2E). The striatum is not uniform and has distinct neurochemical

compositions and connections that are referred to as matrix and striosomes. The similar but more complex compartmentation was reported in the human Acb [47]. We have performed additional immunohistochemistry for tyrosine hydroxylase (TH) and tau in serially-cut, free-floating sections in two TPD cases, in which the remnants of Acb blocks were available after the initial sectioning for the main body of this study. Comparison of the adjacent sections stained for TH and tau indicates that tau pathology preferentially occurs in areas where the fine, mesh-like TH staining is relatively light (Additional file 4: Figure S3). Such a result suggests the relationship between the uneven distribution of tau pathology and neurochemical heterogeneity in the Acb. However, because of the limited number of currently available samples and of the more complex neurochemical architecture in the Acb than the simple matrix-striosome structure in the caudate nucleus [47], future, extensive studies should be needed for further exploration.

Conclusions

We have found frequent tau accumulation in the Acb in patients with TPD. Both the medium-sized and large neurons are affected. While similar tau accumulation was seen in a small number of all AD patients, it was far more frequent and consistent in TPD than AD. The tau isoforms abnormally accumulated in the Acb were 3R and 4R, which suggests a common origin with the hippocampal tau pathology. The Acb receives direct and massive projections from the hippocampal CA1 and subiculum where tau pathology is extremely severe in TPD. Such a result may support the idea that abnormal tau aggregation propagates via neural circuits. Tau accumulation in TPD should be a subject of further investigations to approach the long-lasting issue of the simultaneous deposition of Aβ and tau in AD. In addition, the relationship between the tau pathology in the Acb and such psychiatric symptoms as delusion in TPD needs further exploration.

Additional files

Additional file 1: Table S1. The primary antibodies used in this study.

Additional file 2: Figure S1. Tau accumulation in the Acb in AD and non-demented, aged subjects. Immunohistochemistry with AT8. A: absence of tau positive neurons in an AD case in Braak and Braak's NFT stage IV. Scale bar = 100 μm in A-C. B: a diffuse cytoplasmic staining, neuropil threads and duystrophic neurite in a senile plaque in an AD case in NFT stage VI. C: a tau positive neuron and neuropil threads in a non-demented, aged subject.

Additional file 3: Figure S2. A graph of the density of neuronal tau accumulation in the Acb. The left plots: the group of Braaks' NFT stages III and IV, which includes non-demented aged subjects, TPD cases and AD cases with Braaks' NFT stage IV. Cases with delusion in the clinical history show higher tau score than those without delusion in the Acb. The right plots: the group of AD cases with Braaks' NFT stages IV through VI. Again, cases with delusion show higher tau score than those without delusion.

Additional file 4: Figure S3. The serial section immunohistochemistry for tau and tyrosine hydroxylase (TH). Forty micrometer thick, free floating sections were cut serially from two tangle predominant dementia (TPD) cases, in which the remnants of Acb blocks were available after the initial sectioning for the main body of the study. A set of every other section was stained for TH and the other set for tau with AT8. A and C: AT8 staining in a TPD case 1. B: TH staining of the section between A and C. In B, two types of areas are distinguished based on the modest difference in the density of fine, mesh-like TH staining. There is a propensity that tau pathology preferentially occurs in areas where the fine, mesh-like TH staining is relatively light (A, C). Scale bar = 2 mm in A (A, B and C are at the same magnification). D: higher power photomicrographs of the boxed areas in B and C. The left half is the staining with AT8 and the right half staining for TH. Scale bar = 400 micro-m (D).

Abbreviations

(TPD): Tangle-predominant dementia; (NFT): Neurofibrillary tangles; (AD): Alzheimer's disease; (3R): 3-repeat; (4R): 4-repeat; (Acb): Nucleus accumbens; (VTA): Ventral tegmental area; (HE): Hematoxylin and eosin; (PFA): Paraformaldehyde; (PHF): Paired helical filaments; (Aβ): Amyloid β protein; (TH): tyrosine hydroxylase.

Competing interests

The authors declare that they have no competing interests.

Authors' contributions

IK carried out the microscopic observation, immunoblot and statistical analyses. IK also drafted the initial manuscript. MHa conducted the sample preparation and immunoblot and carried them out with IK. TA participated in the design and coordination of the study. KI carried out the microscopic observation with IK. KO, KN and NA organized the brain archives including clinical information, selected appropriate cases, and performed neuropathological analyses of all cases used in this study. OK participated in the design of the study and performed statistical analyses with IK. SH conceived of the study and participated in the initial design. MHo contributed to the reagents, materials and analysis tools, and conducted free-floating immunohistochemistry. YH participated in the design of the study and helped to draft the manuscript. HA supervised the design and coordination of the study and worked up the manuscript. All authors read and approved the final manuscript.

Authors' information

IK is a graduate student of Department of Psychiatry, Graduate school of Medicine, Yokohama City University School of Medicine. MHa is the senior director of Department of Neuropathology and Cell Biology, Tokyo Metropolitan Institute of Medical Science (TMIMS). TA, KI, NA and SH contributed to this study as visiting scientists of Dementia project, TMIMS. TA is also an associated professor of Department of Psychiatry, Graduate School of Comprehensive Human Sciences, University of Tsukuba. KO and KN are psychiatrists and neuropathologists in Tokyo Metropolitan Matsuzawa Hospital (TMMH), visiting scientists of Dementia project, TMIMS and in charge of the brain archive of TMMH/TMIMS. OK is an associate professor of Department of Psychiatry, Graduate school of Medicine, Yokohama City University School of Medicine. MHo is a chief researcher of Dementia project, TMIMS. YH is a professor of Department of Psychiatry, Graduate school of Medicine, Yokohama City University School of Medicine. HA is the senior director of Dementia project, TMIMS.

Acknowledgements

We are grateful to the patients and their families who made this research possible. We thank Dr. Peter Davies (Albert Einstein College of Medicine) for providing us with his excellent anti-tau antibodies, PHF-1 and MC-1. We also thank Ms. Yoko Shimomura and Mr. Kentaro Endo (Tokyo Metropolitan Institute of Medical Science) for their technical assistance with immuno-electron microscopy, and Ms. Yoko Shimomura, Ms. Hiromi Kondo and Ms. Chie Haga (Tokyo Metropolitan Institute of Medical Science) for their assistance in tissue preparation and staining. Helpful advice by Dr. Takashi Nonaka (Tokyo Metropolitan Institute of Medical Science), as well as Dr. Takashi Togo and Dr. Masatake Uchikado (Department of Psychiatry, Yokohama City University School of Medicine), is very much appreciated. None of the

authors has any conflict of interest. This research was supported by Grants-in-Aid from the Ministry of Health, Labor and Welfare (12946221, MH, MH and HA) and Ministry of Education, Culture, Science (24500429, HA), Japan.

Author details
[1]Dementia Research Project, Tokyo Metropolitan Institute of Medical Science, 2-1-6 Kamikitazawa, Setagaya-ku, Tokyo 156-8506, Japan. [2]Department of Psychiatry, Graduate school of Medicine, Yokohama City University School of Medicine, Yokohama, Japan. [3]Department of Neuropathology and Cell Biology, Tokyo Metropolitan Institute of Medical Science, Tokyo, Japan. [4]Department of Psychiatry, Graduate School of Comprehensive Human Sciences, University of Tsukuba, Tsukuba, Japan. [5]Department of inflammation of Pathology, Faculty of Medicine, Kagawa University, Takamatsu, Japan. [6]Tokyo Metropolitan Matsuzawa Hospital, Tokyo, Japan.

Received: 16 February 2014 Accepted: 1 April 2014
Published: 8 April 2014

References

1. Ikeda K, Akiyama H, Arai T, Oda T, Kato M, Iseki E, Kosaka K, Wakabayashi K, Takahashi H (1999) Clinical aspects of 'senile dementia of the tangle type'- a subset of dementia in the senium separable from late onset. Alzheimer's disease. Dement Geriatr Cogn Disord 10:6–11
2. Noda K, Sasaki K, Fujimi K, Wakisaka Y, Tanizaki Y, Wakug- awa Y, Kiyohara Y, Iida M, Aizawa H, Iwaki T (2006) Quantitative analysis of neurofibrillary pathology in a general population to reappraise neuropathological criteria for senile dementia of the neurofibrillary tangle type (tangle-only dementia) the Hisayama Study. Neuropathology 26:508–518
3. Jellinger KA, Attems J (2007) Neurofibrillary tangle-predominant dementia: comparison with classical Alzheimer disease. Acta Neuropathol 113:107–117
4. McKhann GM, Albert MS, Grossman M, Miller B, Dickson D, Trojanowski JQ, Work Group on Frontotemporal Dementia and Pick's Disease (2001) Clinical and pathological diagnosis of frontotemporal dementia: report of the work group on frontotemporal dementia and Pick's disease. Arch Neurol 58:1803–1809
5. Cairns NJ, Bigio EH, Mackenzie IR, Neumann M, Lee VM, Hatanpaa KJ, White CL 3rd, Schneider JA, Grinberg LT, Halliday G, Duyckaerts C, Lowe JS, Holm IE, Tolnay M, Okamoto K, Yokoo H, Murayama S, Woulfe J, Munoz DG, Dickson DW, Ince PG, Trojanowski JQ, Mann DM (2007) Neuropathologic diagnostic and nosologic criteria for frontotemporal lobar degeneration: consensus of the Consortium for Frontotemporal Lobar Degeneration. Acta Neuropathol 114:5–22
6. Braak H, Braak E (1991) Neuropathological staging of Alzheimer-related changes. Acta Neuropathol 82:239–259
7. Yamada M (2003) Senile dementia of the neurofibrillary tangle type (tangle-only dementia): neuropathological criteria and clinical guidelines for diagnosis. Neuropathology 23:311–317
8. Kovacs GG, Molnár K, László L, Ströbel T, Botond G, Hönigschnabl S, Reiner-Concin A, Palkovits M, Fischer P, Budka H (2011) A peculiar constellation of tau pathology defines a subset of dementia in the elderly. Acta Neuropathol 122:205–222
9. Groenewegen HJ, Vermeulen-Van der Zee E, te Kortschot A, Witter MP (1987) Organization of the projections from the subiculum to the ventral striatum in the rat. A study using anterograde transport of Phaseolus vulgaris leucoagglutinin. Neuroscience 23:103–210
10. Kita H, Kitai ST (1990) Amygdaloid projections to the frontal cortex and the striatum in the rat. J Comp Neurol 298:40–49
11. Berendse HW, Galis-de Graaf Y, Groenewegen HJ (1992) Topographical organization and relationship with ventral striatal compartments of prefrontal corticostriatal projections in the rat. J Comp Neurol 316:314–347
12. French SJ, Totterdell S (2002) Hippocampal and prefrontal cortical inputs monosynaptically converge with individual projection neurons of the nucleus accumbens. J Comp Neurol 446:151–165
13. Heimer L, Zahm DS, Churchill L, Kalivas PW, Wohltmann C (1991) Specificity in the projection patterns of accumbal core and shell in the rat. Neuroscience 41:89–125
14. Groenewegen HJ, Berendse HW, Meredith GE, Haber SN, Voorn P, Wolters JG, Lohman AHM (1991) Functional anatomy of the ventral limbic system-innervated striatum. In: Willner P, Scheel-Kruger J (eds) The mesolimbic dopamine system: from motivation to action. Wiley, Chichester, pp 19–59
15. Rahman S, McBride WJ (2001) D1-D2 dopamine receptor interaction within the nucleus accumbens mediates long-loop negative feedback to the ventral tegmental area (VTA). J Neurochem 77:1248–1255
16. Kalivas PW, Nakamura M (1999) Neural systems for behavioral activation and reward. Curr Opin Neurobiol 9:223–227
17. Cardinal RN, Parkinson JA, Hall J, Everitt BJ (2002) Emotion and motivation: the role of the amygdala, ventral striatum, and prefrontal cortex. Neurosci Biobehav Rev 26:321–352
18. Grace AA, Bunney BS, Moore H, Todd CL (1997) Dopamine-cell depolarization block as a model for the therapeutic actions of antipsychotic drugs. Trends Neurosci 20:31–37
19. Grace AA (2000) Gating of information flow within the limbic system and the pathophysiology of schizophrenia. Brain Res Brain Res Rev 31:330–341
20. Jellinger KA, Bancher C (1998) Senile dementia with tangles (tangle predominant form of senile dementia). Brain Pathol 8:367–376
21. Mirra SS, Heyman A, McKeel D, Sumi SM, Crain BJ, Brownlee LM, Vogel FS, Hughes JP, van Belle G, Berg L (1991) The Consortium to Establish a Registry for Alzheimer's Disease (CERAD). Part II. Standardization of the neuropathologic assessment of Alzheimer's disease. Neurology 41:479–486
22. McKeith IG, Dickson DW, Lowe J, Emre M, O'Brien JT, Feldman H, Cummings J, Duda JE, Lippa C, Perry EK, Aarsland D, Arai H, Ballard CG, Boeve B, Burn DJ, Costa D, Del Ser T, Dubois B, Galasko D, Gauthier S, Goetz CG, Gomez-Tortosa E, Halliday G, Hansen LA, Hardy J, Iwatsubo T, Kalaria RN, Kaufer D, Kenny RA, Korczyn A, et al (2005) Diagnosis and management of dementia with Lewy bodies. Third report of the DLB consortium. Neurology 65:1863–18725
23. Aoki N, Higashi S, Kawakami I, Kobayashi Z, Hosokawa M, Katsuse O, Togo T, Hirayasu Y, Akiyama H (2012) Localization of fused in sarcoma (FUS) protein to the post-synaptic density in the brain. Acta Neuropathol 124:383–394
24. Sun A, Nguyen XV, Bing G (2002) Comparative analysis of an improved thioflavin-s stain, Gallyas silver stain, and immunohistochemistry for neurofibrillary tangle demonstration on the same Sections. J Histochem Cytochem 50:463–472
25. Arai T, Ikeda K, Akiyama H, Nonaka T, Hasegawa M, Ishiguro K, Iritani S, Tsuchiya K, Iseki E, Yagishita S, Oda T, Mochizuki A (2004) Identification of amino-terminally cleaved tau fragments that distinguish progressive supranuclear palsy from corticobasal degeneration. Ann Neurol 55:72–79
26. Yamada M, Itoh Y, Sodeyama N, Suematsu N, Otomo E, Matsushita M, Mizusawa H (2001) Senile dementia of the neurofibrillary tangle type: a comparison with Alzheimer's disease. Dement Geriatr Cogn Disord 12:117–126
27. Bancher C, Jellinger KA (1994) Neurofibrillary tangle pre- dominant form of senile dementia of Alzheimer type: a rare subtype in very old subjects. Acta Neuropathol 88:565–570
28. Iseki E, Tsunoda S, Suzuki K, Takayama N, Akatsu H, Yamamoto T, Kosaka K (2002) Regional quantitative analysis of NFT in brains of non-demented elderly persons: comparisons with findings in brains of late-onset Alzheimer's disease and limbic NFT dementia. Neuropathology 22(1):34–39
29. Saito Y, Ruberu NN, Sawabe M, Arai T, Tanaka N, Kakuta Y, Yamanouchi H, Murayama S (2004) Staging of argyrophilic grains: an age-associated tauopathy. J Neuropathol Exp Neurol 63:911–918
30. Ikeda K, Akiyama H, Arai T, Sahara N, Mori H, Usami M, Sakata M, Mizutani T, Wakabayashi K, Takahashi H (1997) A subset of senile dementia with high incidence of the apolipoprotein E epsilon2 allele. Ann Neurol 41:693–695
31. Santa-Maria I, Haggiagi A, Liu X, Wasserscheid J, Nelson PT, Dewar K, Clark LN, Crary JF (2012) The MAPT H1 haplotype is associated with tangle-predominant dementia. Acta Neuropathol 124:693–704
32. Janocko NJ, Brodersen KA, Soto-Ortolaza AI, Ross OA, Liesinger AM, Duara R, Graff-Radford NR, Dickson DW, Murray ME (2012) Neuropathologically defined subtypes of Alzheimer's disease differ significantly from neurofibrillary tangle-predominant dementia. Acta Neuropathol 124:681–692
33. Oyanagi K, Takahashi H, Wakabayashi K, Ikuta F (1987) Selective involvement of large neurons in the neostriatum of Alzheimer's disease and senile dementia: a morphometric investigation. Brain Res 411:205–211
34. Oyanagi K, Takahashi H, Wakabayashi K, Ikuta F (1991) Large neurons in the neostriatum in Alzheimer's disease and progressive supranuclear palsy. Brain Res 544:221–226
35. Hasegawa M, Watanabe S, Kondo H, Akiyama H, Mann DM, Saito Y, Murayama (2014) 3R and 4R tau isoforms in paired helical filaments in Alzheimer's disease. Acta Neuropathol 127:303–305
36. Oyanagi K, Makifuchi T, Ohtoh T, Chen KM, Gajdusek DC, Chase TN, Ikuta F (1994) The neostriatum and nucleus accumbens in parkinsonism-dementia

complex of Guam: a pathological comparison with Alzheimer's disease and progressive supranuclear palsy. Acta Neuropathol 88:122–128
37. Selden N, Mesulam MM, Geula C (1994) Human striatum: the distribution of neurofibrillary tangles in Alzheimer's disease. Brain Res 648:327–331
38. Kim Y, Spruston N (2012) Target-specific output patterns are predicted by the distribution of regular-spiking and bursting pyramidal neurons in the subiculum. Hippocampus 22:693–706
39. Kelley AE, Domesick VB (1982) The distribution of the projection from the hippocampal formation to the nucleus accumbens in the rat: an anterograde- and retrograde-horseradish peroxidase study. Neuroscience 7:2321–2335
40. Weinberger DR, Lipska BK (1995) Cortical maldevelopment, anti-psychotic drugs, and schizophrenia: a search for common ground. Schizophr Res 16:87–110
41. O'Donnell P, Grace AA (1998) Dysfunctions in multiple interrelated systems as the neurobiological bases of schizophrenic symptom clusters. Schizophr Bull 24:267–283
42. Laruelle M (2000) The role of endogenous sensitization in the pathophysiology of schizophrenia: implications from recent brain imaging studies. Brain Res Brain Res Rev 31:371–384
43. Lewis DA, Levitt P (2002) Schizophrenia as a disorder of neurodevelopment. Annu Rev Neurosci 25:409–432
44. Braak H, Zetterberg H, del Tredici K, Blennow K (2013) Intraneuronal tau aggregation precedes diffuse plaque deposition, but amyloid-β changes occur before increases of tau in cerebrospinal fluid. Acta Neuropathol 126:631–641
45. Farber NB, Rubin EH, Newcomer JW, Kinscherf DA, Miller JP, Morris JC, Olney JW, McKeel DW Jr (2000) Increased neocortical neurofibrillary tangle density in subjects with Alzheimer disease and psychosis. Arch Gen Psychiatry 57:1165–1173
46. Togo T, Isojima D, Akatsu H, Suzuki K, Uchikado H, Katsuse O, Iseki E, Kosaka K, Hirayasu Y (2005) Clinical features of argyrophilic grain disease: a retrospective survey of cases with neuropsychiatric symptoms. Am J Geriatr Psychiatry 13:1083–1091
47. Holt DJ, Graybiel AM, Saper CB (1997) Neurochemical architecture of the human striatum. J Comp Neurol 384:1–25

doi:10.1186/2051-5960-2-40
Cite this article as: Kawakami *et al.*: Tau accumulation in the nucleus accumbens in tangle-predominant dementia. *Acta Neuropathologica Communications* 2014 **2**:40.

J Neuropathol Exp Neurol

Vol. 74, No. 2
February 2015
pp. 158–165

ORIGINAL ARTICLE

Progranulin Reduction Is Associated With Increased Tau Phosphorylation in P301L Tau Transgenic Mice

Masato Hosokawa, PhD, Tetsuaki Arai, MD, PhD, Masami Masuda-Suzukake, PhD, Hiromi Kondo, Takashi Matsuwaki, DVM, PhD, Masugi Nishihara, DVM, PhD, Masato Hasegawa, PhD, and Haruhiko Akiyama, MD, PhD

Abstract

Granulin (*GRN*) mutations have been identified in familial frontotemporal lobar degeneration patients with ubiquitin pathology. *GRN* transcript haploinsufficiency is proposed as a disease mechanism that leads to the loss of functional progranulin (PGRN) protein. Thus, these mutations are strongly involved in frontotemporal lobar degeneration pathogenesis. Moreover, recent findings indicate that *GRN* mutations are associated with other neurodegenerative disorders with tau pathology, including Alzheimer disease and corticobasal degeneration. To investigate the potential influence of a decline in PGRN protein on tau accumulation, P301L tau transgenic mice were interbred with *GRN*-deficient mice, producing P301L tau transgenic mice harboring the *GRN* hemizygote. Brains were collected from 13- and 19-month-old mice, and sequential extraction of proteins, immunoblotting, and immunohistochemical analyses were performed. Immunoblotting analysis revealed that tau phosphorylation was accelerated in the Tris-saline soluble fraction of 13-month-old and in the sarkosyl-insoluble fraction of 19-month-old P301L tau/*GRN* hemizygotes compared with those in fractions from P301L tau transgenic mice. Activity of cyclin-dependent kinases was also upregulated in the brains of P301L tau/*GRN* hemizygote mice. Although the mechanisms involved in these findings remain unknown, our data suggest that a reduction in PGRN protein might contribute to phosphorylation and intraneuronal accumulation of tau.

Key Words: Alzheimer disease, Granulin, Phosphorylation, Progranulin, Tau.

INTRODUCTION

Progranulin (PGRN) is a growth factor that is encoded by a single gene on chromosome 17q21. It is a 593-amino acid cysteine-rich protein with a signal peptide (17 amino acids) and highly conserved 7.5 tandem granulin repeats of a 12-cysteinyl motif. It is involved in the regulation of multiple functions, including neuronal cell growth (1, 2), wound healing (3, 4), and inflammation (5). It has also been strongly linked to tumorigenesis (6). Moreover, PGRN has a chemoattractive effect for microglia (7). In 2006, granulin (*GRN*) null mutations were identified in familial frontotemporal dementia linked to chromosome 17q21 with tau-negative ubiquitin-positive inclusions. *GRN* is located in 1.7 Mb centromeric of the *MAPT* (tau) gene (8, 9). Many mutations, including frame shift by insertion and deletion or substitution of a nucleotide that generate premature termination codons, have been reported. *GRN* transcript haploinsufficiency has been proposed as the disease mechanism that leads to the loss of functional PGRN protein. Premature stop codons are not translated into the mutant transcript because translation is blocked by nonsense-mediated RNA decay. The mutation in the signal peptide may cause mislocalization of PGRN in a protein secretion pathway or PGRN loss of function by impairment of PGRN transport (10, 11). Thus, these mutations are strongly involved in frontotemporal dementia pathogenesis.

Loss-of-function GRN mutations have been confirmed in patients clinically diagnosed as having Alzheimer disease (AD) (12–18). Of these, R535X (c.1603 C > T) and Null (IVS0 +5G > C) mutations were originally identified in frontotemporal lobar degeneration (FTLD)-GRN but were also found in AD (12). Two further mutations found in AD, p.Cys139Arg (c.415 T > C) and p.Pro451Leu (c.1352C > T), were indicated to be pathogenic based on evolutionary conservation and silico protein modeling (19). Mutations, p.Gly35Arg (c.103G > A) (20), and a single base pair deletion (c. 154delA) were also found in AD, and the latter was shown to cause a frame shift (p.Thr52HisfsX2), creating a premature

From the Dementia Research Project (MH, TA, HA), Department of Neuropathology and Cell Biology (MM-S, MH), and Histology Center (HK), Tokyo Metropolitan Institute of Medical Science, Setagaya-ku, Tokyo; Department of Neuropsychiatry, Division of Clinical Medicine, Faculty of Medicine, University of Tsukuba, Tsukuba, Ibaraki (TA); and Department of Veterinary Physiology, Graduate School of Agricultural and Life Sciences, The University of Tokyo, Bunkyo-ku, Tokyo (TM, MN), Japan.

Send correspondence and reprint requests to: Masato Hosokawa, PhD, Dementia Research Project, Tokyo Metropolitan Institute of Medical Science, 2-1-6, Kamikitazawa, Setagaya-ku, Tokyo 156-8506, Japan; E-mail: hosokawa-ms@igakuken.or.jp

Masami Masuda-Suzukake, PhD, is now with Medical Research Council, Laboratory of Molecular Biology, Neurobiology Division, Francis Crick Ave, Cambridge Biomedical Campus, Cambridge, CB2 0QH, UK.

This research was partially supported by the Japan Society for the Promotion of Science, Grant-in-Aid for Scientific Research (C) (JSPS KAKENHI grant 21591536 to Haruhiko Akiyama and 24591738 to Masato Hosokawa). Additional funding for our study was supplied by our institute.

Conflict of interest statement: None declared.

Supplemental digital content is available for this article. Direct URL citations appear in the printed text and are provided in the HTML and PDF versions of this article on the journal's Web site (www.jneuropath.com).

stop codon (21). The rs5848 (3′UTR +78C > T) variant in the 3′ untranslated region (UTR) of *GRN* is known to reduce *GRN* mRNA levels in the brain and peripheral mononuclear cells in patients. The rs5848 variant was also found in AD (22) and is associated with a risk for AD (23). Granulin mutations have also been found in another tauopathy, corticobasal syndrome (24); they include a novel splice donor site mutation in the *GRN* gene p.Val200GlyfsX18 (IVS7+1G > A) (25), pVal279GlyfsX5 (IVS8-G > C) (10), p.Thr272SerfsX10 (c.813_816delCACT) (26), and p.Ala9Asp (c.26C > A) (27). Furthermore, tau pathology, in addition to TDP-43 pathology, was reported to be found in most patients in 2 families harboring a *GRN* mutation (28).

These findings suggest that the decline or dysfunction of PGRN may contribute to tau abnormalities that lead to tau pathology by an unknown mechanism. To elucidate these issues, we produced P301L tau transgenic mice harboring the *GRN* hemizygote (Tau/$GRN^{+/-}$) by interbreeding P301L tau transgenic mice with *GRN*-deficient mice and analyzed whether the *GRN* reduction affects phosphorylation and intracellular accumulation of tau.

MATERIALS AND METHODS

Ethics Statement

This study was carried out in strict accordance with the recommendations provided in the Guide for the Care and Use of Laboratory Animals of the Ministry of Health, Labour and Welfare of Japan and the Ministry of Education, Culture, Sports, Science and Technology of Japan. The protocol was approved by the Committee on the Ethics of Animal Experiments of the Tokyo Metropolitan Institute of Medical Science (Permit No. 22-23 and 11-028). All experiments were performed under sodium pentobarbital or isoflurane anesthesia, and every effort was made to minimize suffering.

Animals

P301L tau transgenic mice (JNPL3) (29) were purchased from Taconic (Hudson, NY) via IBL (Gunma, Japan). Granulin (*GRN*)-deficient (knockout [KO]) mice were obtained from RIKEN Bioresource Center (Tsukuba, Japan), which was established by Kayasuga et al (30). *GRN*-KO mice had been backcrossed to C57BL/6 J mice for more than 10 generations. Male P301L tau homozygote transgenic mice were interbred with female *GRN*-KO mice, or female P301L tau homozygote transgenic mice were interbred with male *GRN*-KO mice. P301L tau transgenic mice harboring the *GRN* hemizygote (Tau/$GRN^{+/-}$) were produced. Control mice (Tau hemizygote) were produced by interbreeding male P301L tau homozygote transgenic mice and female C57BL/6 J. We used male mice in this study. The mice were reared in the animal facility of Tokyo Metropolitan Institute of Medical Science under conventional conditions at 24°C ± 2°C and were maintained on a commercial diet (CE-2; Nihon CLEA, Shizuoka, Japan) ad libitum.

Mice were killed under quick anesthesia with isoflurane (Mylan Pharmaceutical Company, Tokyo, Japan), and the brains were quickly removed. Brains of each group were cut in the sagittal plane; the left hemispheres were frozen and stored at −80°C for biochemical analyses. The right hemispheres were fixed in 4% paraformaldehyde in 0.1 mol/L phosphate buffer for 48 hours in the cold. Brain blocks were then transferred to a maintenance solution of 20% sucrose in 0.01 mol/L PBS, pH 7.4.

Sequential Fractionation of Brain Extracts

Frozen left hemispheres (~0.2 g) were homogenized in 10 volumes of buffer H (10 mmol/L Tris-HCl, pH 7.5; 0.8 mol/L NaCl; 1 mmol/L ethylene glycol bis-N,N,N′,N′-tetraacetic acid; 1 mmol/L dithiothreitol). The hemisphere included the olfactory bulb, cerebral cortex, striatum, thalamus, hypothalamus, cerebellum, midbrain, pons, medulla oblongata, and the upper part of the spinal cord. The method used for sequential fractionation of brain extracts was originally described by Greenberg and Davies (31). Briefly, each brain homogenate was centrifuged at 100,000 × *g* for 20 minutes at 4°C; the supernatant was then collected as the Tris-soluble fraction. The resultant pellet was homogenized in 10 volumes of buffer H, followed by an incubation for 30 minutes at 37°C with 1% Triton X-100. The homogenate was then centrifuged at 100,000 × *g* for 20 minutes at 4°C. The Triton X-100 insoluble pellet was sonicated in 5 volumes of buffer H, followed by incubation for 30 minutes at 37°C with 1% sarkosyl and centrifuged at 100,000 × *g* for 20 minutes at 4°C. The pellet was sonicated in 1 volume of

TABLE 1. Sources and Dilutions of Primary Antibodies

Antibody	Type	Source	Dilution
α-tubulin	Mouse mAb	Sigma, St. Louis, MO	1:10,000
AT8	Mouse mAb	Innogenetics, Gent, Belgium	1:2000
HT7	Mouse mAb	Innogenetics	1:3000
T46	Mouse mAb	Zymed/Invitrogen, Camarillo, CA	1:3000
pT181	Rabbit pAb	Biosource International, Thermo Fisher Scientific, Waltham, MA	1:2000
pS422	Rabbit pAb	Biosource or Dr Hasegawa	1:2000
phosphor-Akt substrate	Rabbit mAb	Cell Signaling, Danvers, MA	1:1000
phosphor-(Ser) CDKs substrate	Rabbit pAb	Cell Signaling	1:1000
phospho-(Thr) MAPK/CDK substrate	Mouse mAb	Cell Signaling	1:1000
phosphor-PKA substrate	Rabbit mAb	Cell Signaling	1:1000
phosphor-(Ser) PKC substrate	Rabbit pAb	Cell Signaling	1:1000

mAb, monoclonal antibody; pAb, polyclonal antibody.

sodium dodecylsulfate (SDS)–polyacrylamide gel electrophoresis sample buffer.

Immunoblotting Analysis

For immunoblotting, brain extracts from the mice were boiled for 5 minutes with SDS–polyacrylamide gel electrophoresis sample buffer (60 mmol/L Tris-HCl, pH 6.8, containing 2% SDS, 10% glycerol, 0.025% bromophenol blue, and 5% mercaptoethanol) and loaded onto a 10% acrylamide minigel. Loaded samples were electrophoresed for 45 minutes at 200 V with molecular weight markers (Bio-Rad, Hercules, CA). Electrophoresed proteins were transferred onto a polyvinylidene difluoride membrane (Millipore, Billerica, MA) for 60 minutes at 200 mA. The printed membranes were blocked with 3% gelatin for 30 minutes and then incubated in a primary antibody solution (T46, 1:3000; AT8, 1:2000; anti-pT181,

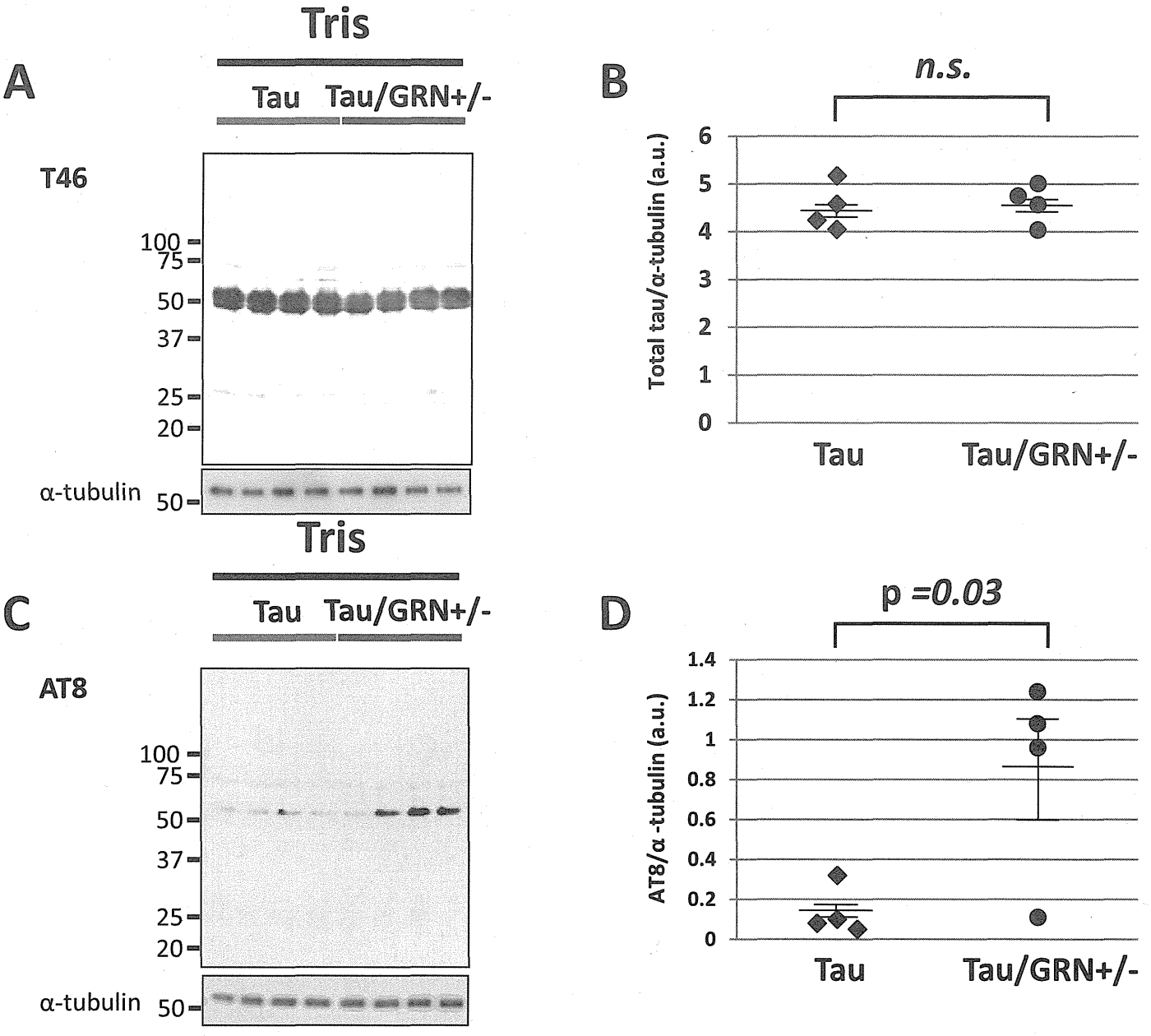

FIGURE 1. Total tau and phosphorylated tau of sequential fractionation protein samples. **(A)** Immunoblotting analysis was visualized using the T46 antibody for detecting total tau in the Tris-soluble fraction of the brains of 13-month-old mice. Four P301L tau mice and four P301L tau/GRN$^{+/-}$ mice were used for this assay. **(B)** A comparison of relative total tau expression levels in the Tris-soluble fraction of 13-month-old mice. The data were compared with the T46 band median intensity/α-tubulin. There was no significant difference between the 2 groups by Student *t*-test. **(C)** Immunoblotting analysis was visualized using AT8 antibody for detecting phosphorylated tau in the Tris-soluble fraction. Molecular weight markers are shown on the left (kDa). **(D)** A comparison of relative phosphorylated tau (AT8) expression levels in the Tris-soluble fraction of 13-month-old mice. The data were compared with the AT8 band median intensity/α-tubulin. $p < 0.05$ was considered significant by Mann-Whitney U test. a.u., arbitrary units.